Reconstruction of Sparse Scatterers through an Approximated Compressive Sensing Strategy

L. Poli, G. Oliveri, A. Massa

Abstract

This report proposes a numerical validation of the Bayesian Compressive Sampling-based technique for imaging dielectric cylinders within the conditions of "sparsity" and "weakness" of the scatterers. Various shake of the scatterers and different values of dielectric permittivity have been considered.

Contents

1 TEST CASE: Two Square Cylinders

Goal: show the performances of BCS when dealing with a sparse scatterer

- Number of Views: V
- Number of Measurements: M
- Number of Cells for the Inversion: N
- Number of Cells for the Direct solver: D
- Side of the investigation domain: L

Test Case Description

Direct solver:

- Square domain divided in $\sqrt{D} \times \sqrt{D}$ cells
- Domain side: $L = 3\lambda$
- $D = 1296$ (discretization for the direct solver: $< \lambda/10$)

Investigation domain:

- Square domain divided in $\sqrt{N} \times \sqrt{N}$ cells
- $L = 3\lambda$
- $2ka = 2 \times \frac{2\pi}{\lambda} \times \frac{L\sqrt{2}}{2} = 6\pi\sqrt{2} = 26.65$
- $\#DOF = \frac{(2ka)^2}{2} = \frac{(2\times\frac{2\pi}{\lambda}\times\frac{L\sqrt{2}}{2})^2}{2} = 4\pi^2 \left(\frac{L}{\lambda}\right)^2 = 4\pi^2 \times 9 \approx 355.3$
- N scelto in modo da essere vicino a $\#DOF$: $N = 324$ (18×18)

Measurement domain:

- Measurement points taken on a circle of radius $\rho = 3\lambda$
- Full-aspect measurements
- $M \approx 2ka \rightarrow M = 27$

Sources:

- Plane waves
- $V \approx 2ka \rightarrow V = 27$
- Amplitude $A = 1$
- Frequency: 300 MHz $(\lambda = 1)$

Object:

- Two square cylinders of side $\frac{\lambda}{6} = 0.1667$
- $\varepsilon_r \in \{1.5, 2.0, 2.5, 3.0\}$ (one square), $\varepsilon_r = 1.9$ (one square)
- $\sigma = 0$ [S/m]

BCS parameters:

- Initial estimate of the noise: $n_0 = 1.0 \times 10^{-3}$
- Convergenze parameter: $\tau = 1.0 \times 10^{-8}$

RESULTS: $\varepsilon_r = 1.5$

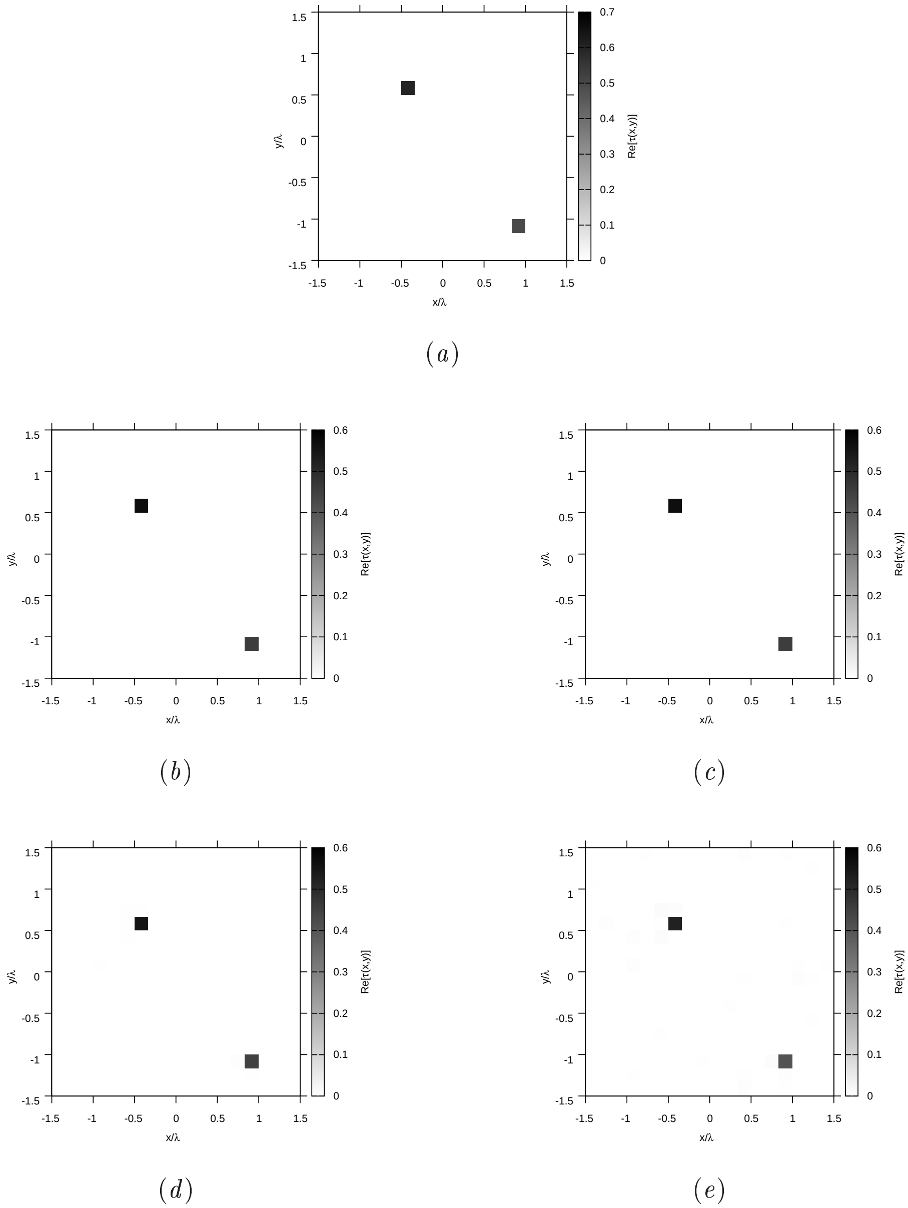

Figure 17. Actual object (a) and BCS reconstructed object for (b) Noiseless case, (c) $SNR = 20$ [dB] , (d) $SNR = 10$ [dB] , (e) $SNR = 5$ [dB].

Observations:

Ricostruzioni molto buone per tutti i valori di SNR.

RESULTS: $\varepsilon_r = 2.0$

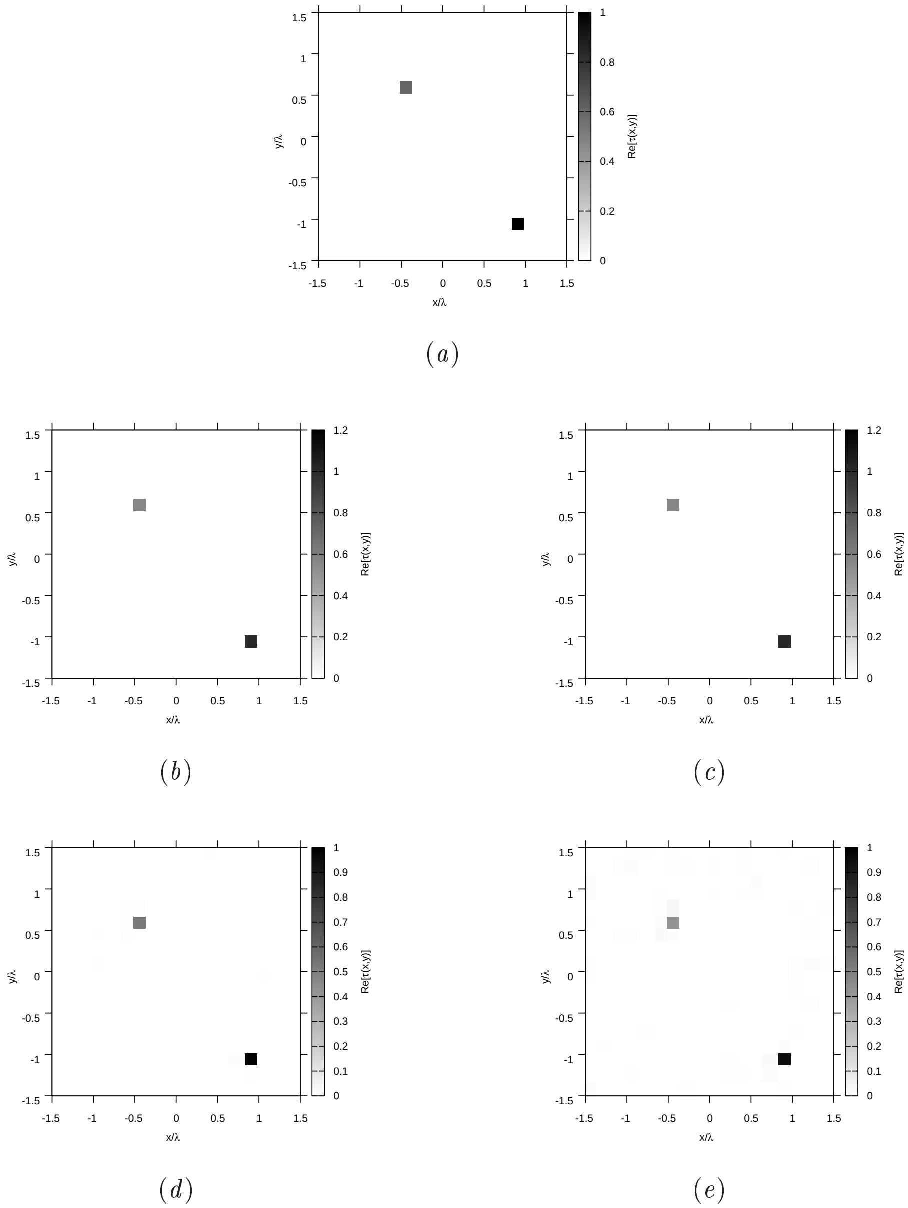

Figure 18. Actual object (a) and BCS reconstructed object for (b) Noiseless case, (c) $SNR = 20$ [dB] , (d) $SNR = 10$ [dB] , (e) $SNR = 5$ [dB].

Observations:

Ricostruzioni in generale buone per tutti i valori di SNR.

RESULTS: $\varepsilon_r = 2.5$

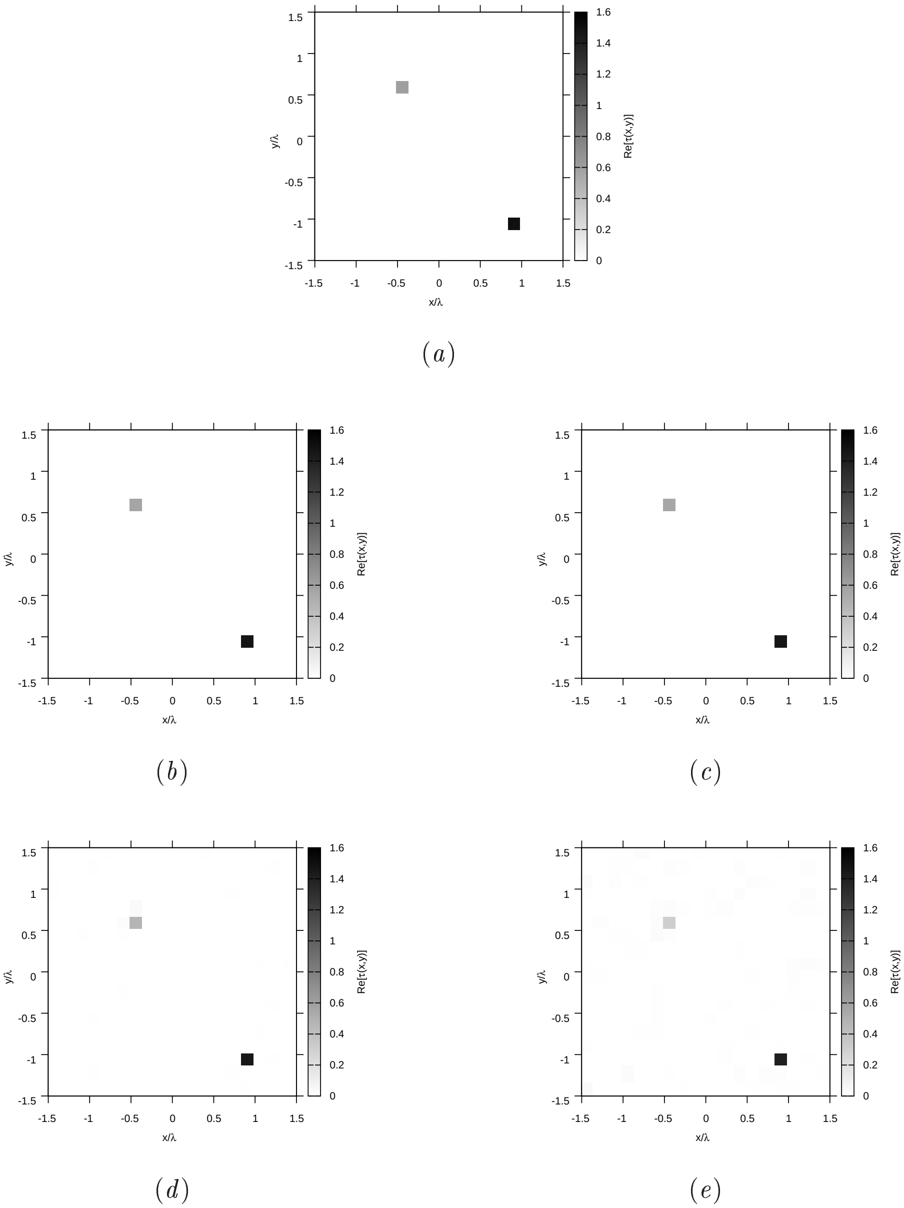

Figure 19. Actual object (a) and BCS reconstructed object for (b) Noiseless case, (c) $SNR = 20$ [dB] , (d) $SNR = 10$ [dB] , (e) $SNR = 5$ [dB].

Observations:

Ricostruzioni in generale buone per tutti i valori di SNR.

RESULTS: $\varepsilon_r = 3.0$

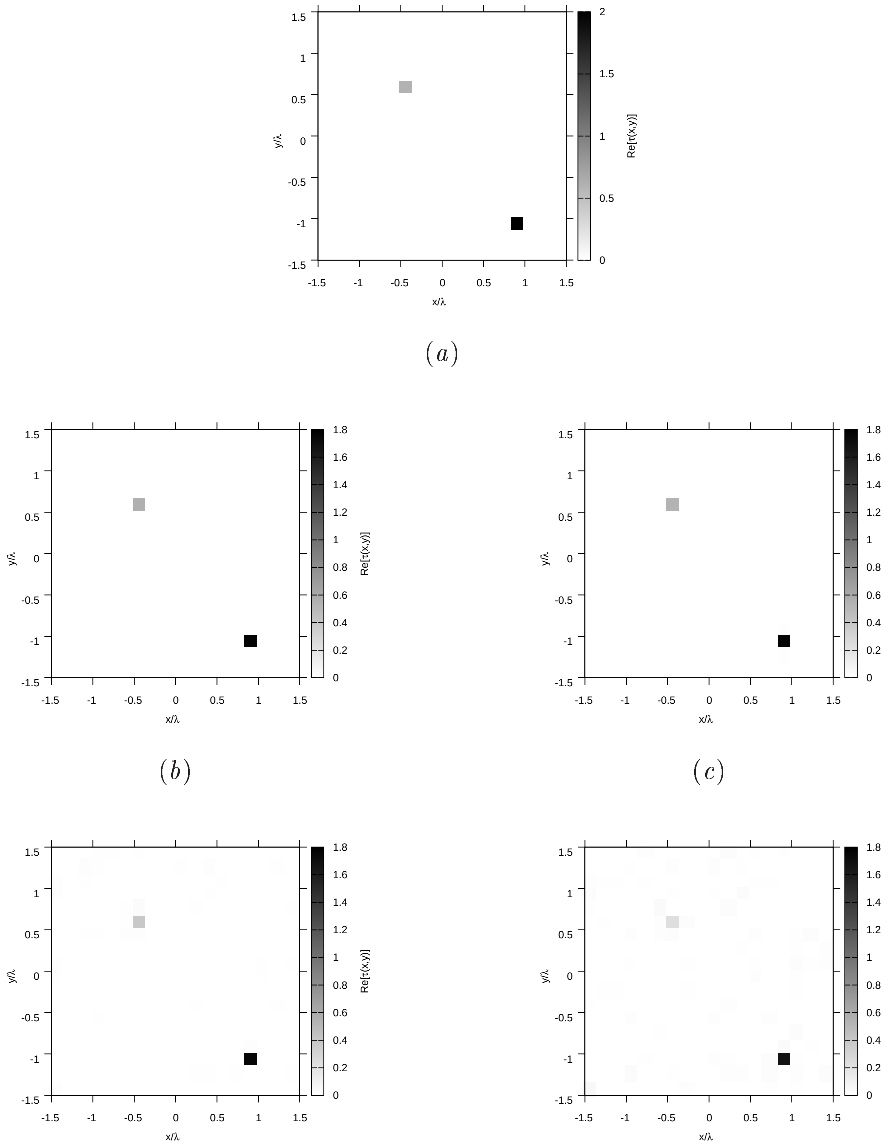

(a) (b) (c) (d) (e)

Figure 20. Actual object (a) and BCS reconstructed object for (b) Noiseless case, (c) $SNR = 20$ [dB] , (d) $SNR = 10$ [dB] , (e) $SNR = 5$ [dB].

Observations:

Ricostruzioni in generale buone per tutti i valori di SNR.

RESULTS: Error Figures

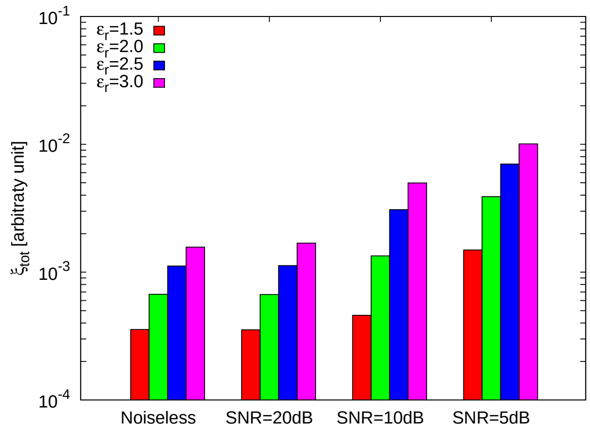

(a)

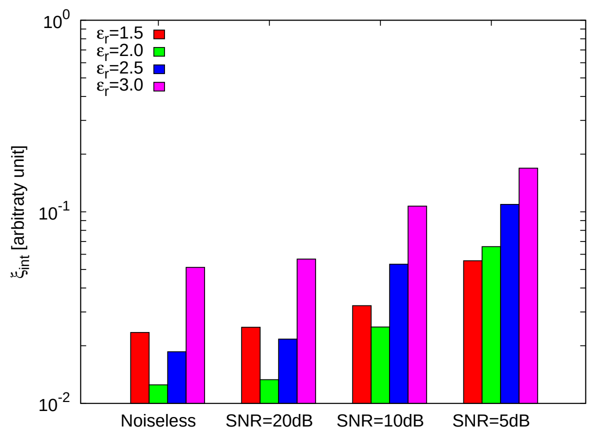

(b)

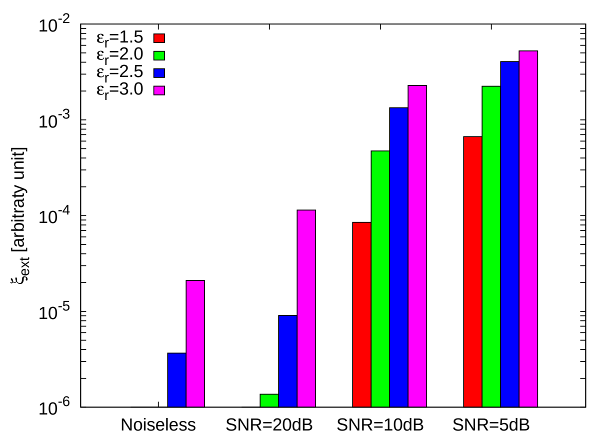

(c)

Figure 21. Behaviour of error figures as a function of ε_r, for different SNR values: (a) total error ξ_{tot}, (b) internal error ξ_{int}, (c) external error ξ_{ext}.

2 TEST CASE: Three Square Cylinders

Goal: show the performances of BCS when dealing with a sparse scatterer

- Number of Views: V
- Number of Measurements: M
- Number of Cells for the Inversion: N
- Number of Cells for the Direct solver: D
- Side of the investigation domain: L

Test Case Description

Direct solver:

- Square domain divided in $\sqrt{D} \times \sqrt{D}$ cells
- Domain side: $L = 3\lambda$
- $D = 1296$ (discretization for the direct solver: $< \lambda/10$)

Investigation domain:

- Square domain divided in $\sqrt{N} \times \sqrt{N}$ cells
- $L = 3\lambda$
- $2ka = 2 \times \frac{2\pi}{\lambda} \times \frac{L\sqrt{2}}{2} = 6\pi\sqrt{2} = 26.65$
- $\#DOF = \frac{(2ka)^2}{2} = \frac{(2\times\frac{2\pi}{\lambda}\times\frac{L\sqrt{2}}{2})^2}{2} = 4\pi^2\left(\frac{L}{\lambda}\right)^2 = 4\pi^2 \times 9 \approx 355.3$
- N scelto in modo da essere vicino a $\#DOF$: $N = 324$ (18×18)

Measurement domain:

- Measurement points taken on a circle of radius $\rho = 3\lambda$
- Full-aspect measurements
- $M \approx 2ka \rightarrow M = 27$

Sources:

- Plane waves
- $V \approx 2ka \rightarrow V = 27$
- Amplitude $A = 1$
- Frequency: 300 MHz $(\lambda = 1)$

Object:

- Three square cylinders of side $\frac{\lambda}{6} = 0.1667$
- $\varepsilon_r \in \{1.5, 2.0, 2.5, 3.0\}$ (two squares), $\varepsilon_r = 1.9$ (one square)
- $\sigma = 0$ [S/m]

BCS parameters:

- Initial estimate of the noise: $n_0 = 1.0 \times 10^{-3}$
- Convergenze parameter: $\tau = 1.0 \times 10^{-8}$

RESULTS: $\varepsilon_r = 1.5$

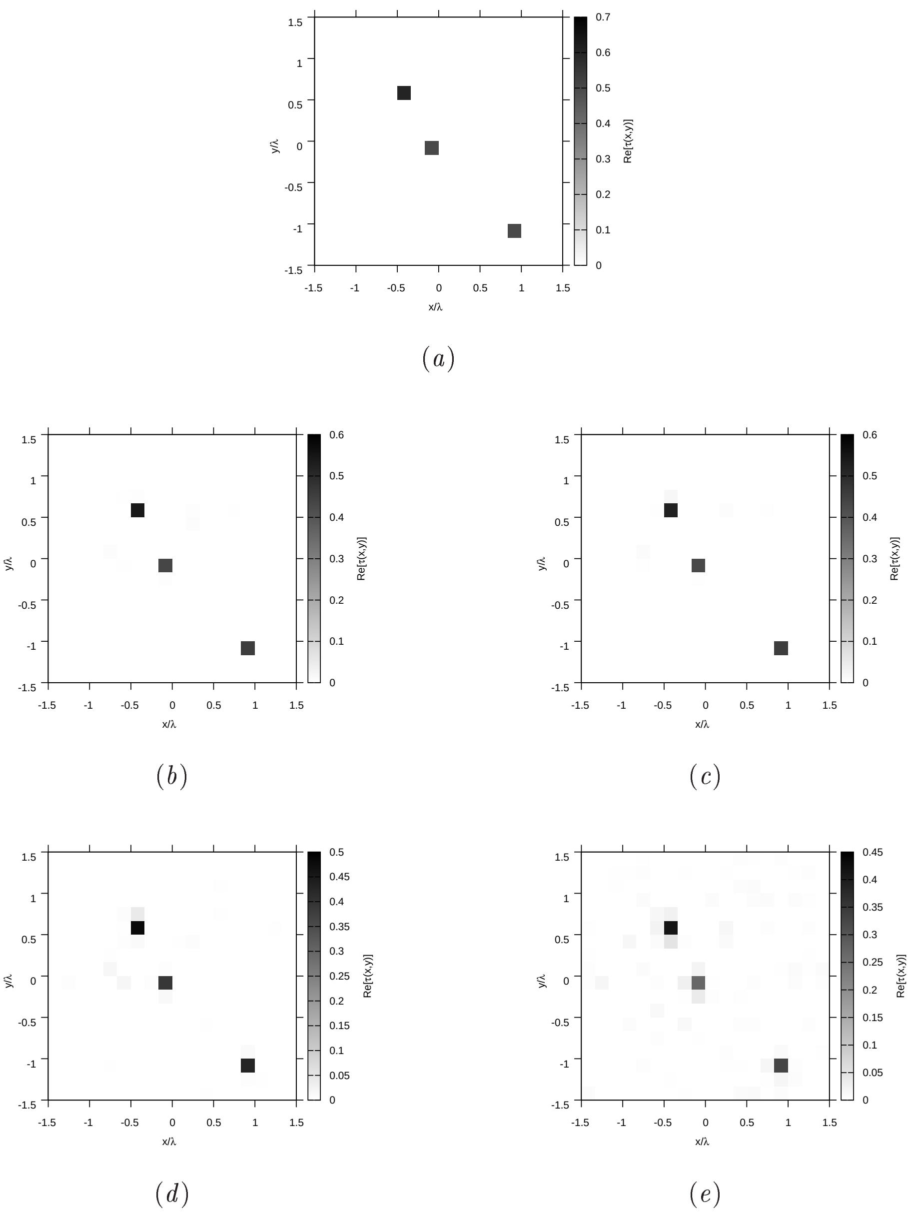

Figure 22. Actual object (a) and BCS reconstructed object for (b) Noiseless case, (c) $SNR = 20$ [dB] , (d) $SNR = 10$ [dB] , (e) $SNR = 5$ [dB].

Observations:

Ricostruzioni molto buone per i casi Noiseless e $SNR = 20\,dB$.

RESULTS: $\varepsilon_r = 2.0$

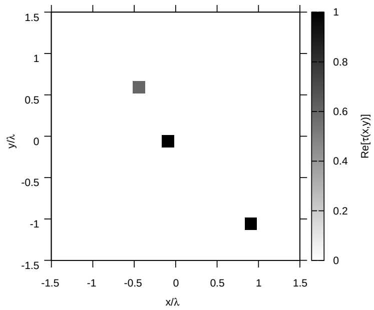

(a)

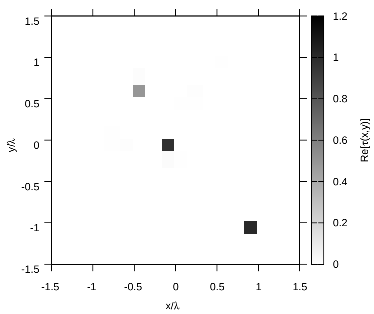

(b)

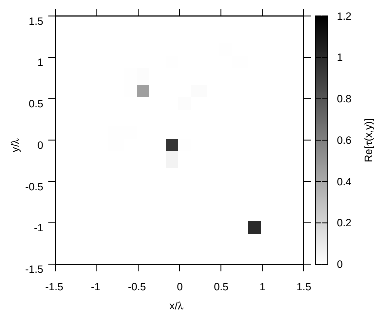

(c)

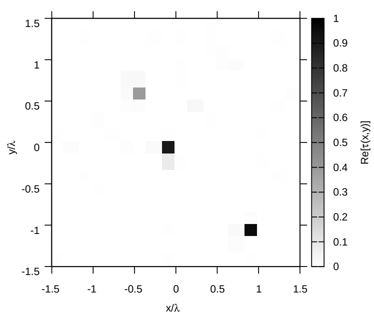

(d)

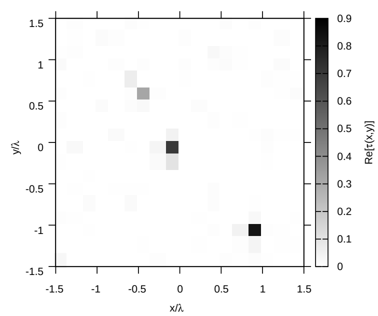

(e)

Figure 23. Actual object (a) and BCS reconstructed object for (b) Noiseless case, (c) $SNR = 20$ [dB] , (d) $SNR = 10$ [dB] , (e) $SNR = 5$ [dB].

Observations:

Ricostruzioni molto buone per i casi Noiseless e $SNR = 20\,dB$.

RESULTS: $\varepsilon_r = 2.5$

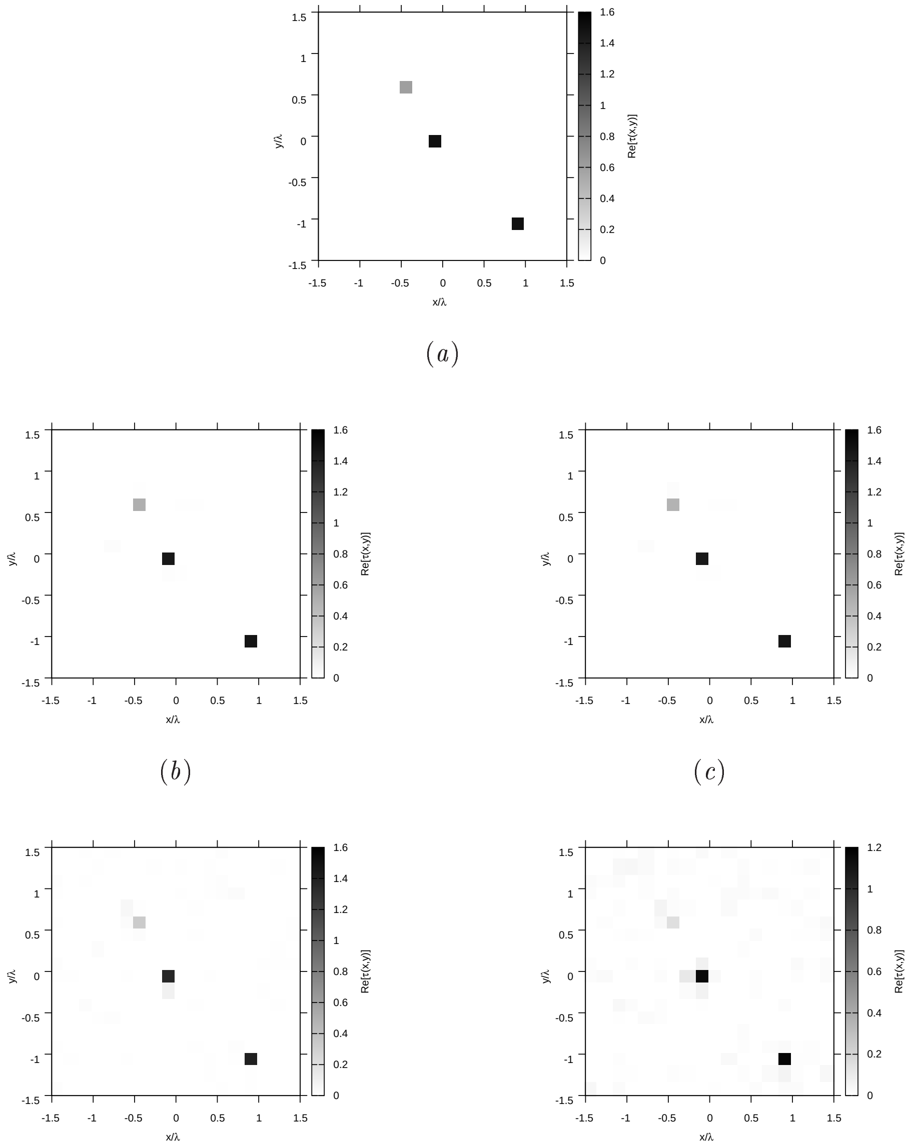

(a)

(b) (c)

(d) (e)

Figure 24. Actual object (a) and BCS reconstructed object for (b) Noiseless case, (c) $SNR = 20$ [dB] , (d) $SNR = 10$ [dB] , (e) $SNR = 5$ [dB].

Observations:

Ricostruzioni molto buone per i casi Noiseless e $SNR = 20\,dB$.

RESULTS: $\varepsilon_r = 3.0$

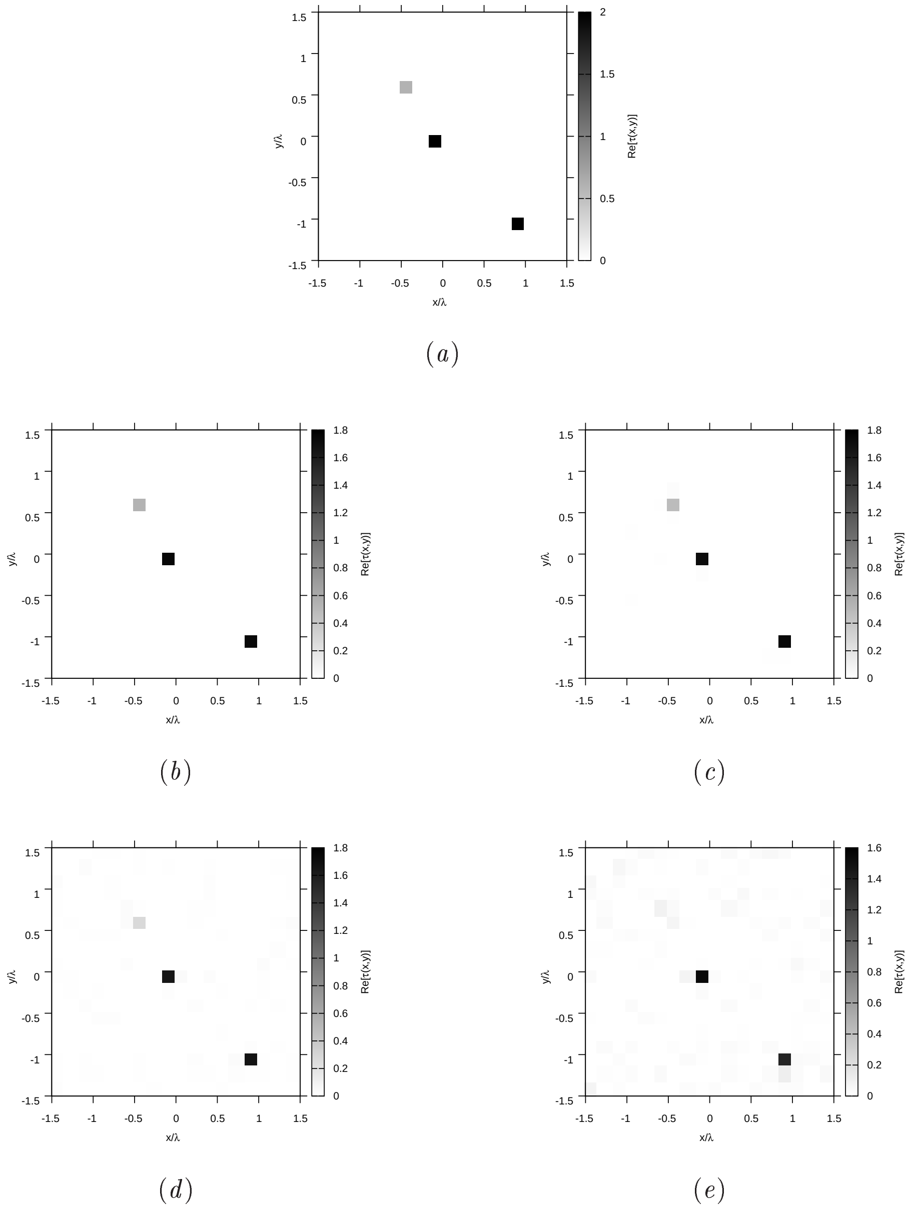

Figure 25. Actual object (a) and BCS reconstructed object for (b) Noiseless case, (c) $SNR = 20$ [dB] , (d) $SNR = 10$ [dB] , (e) $SNR = 5$ [dB].

Observations:

Ricostruzioni molto buone per i casi Noiseless e $SNR = 20\,dB$.

RESULTS: Error Figures

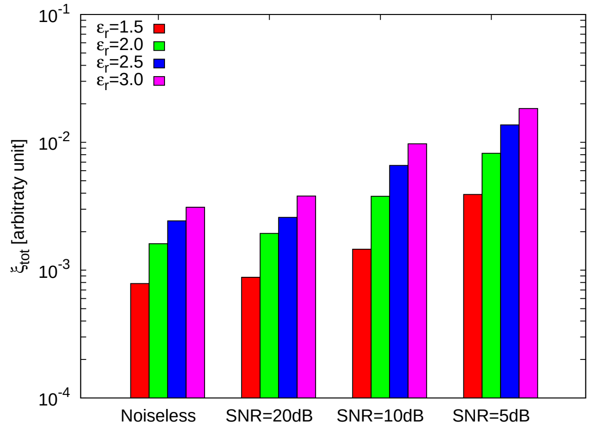

(a)

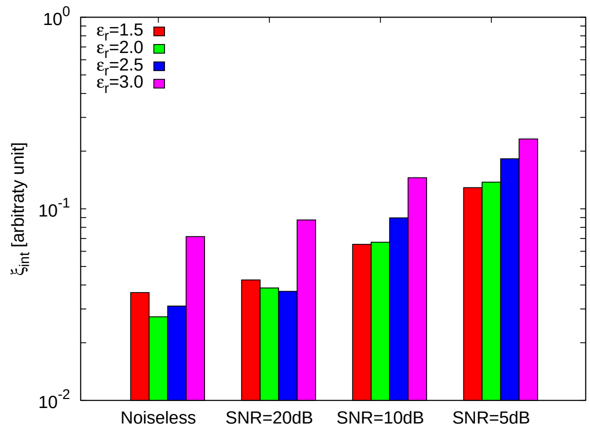

(b)

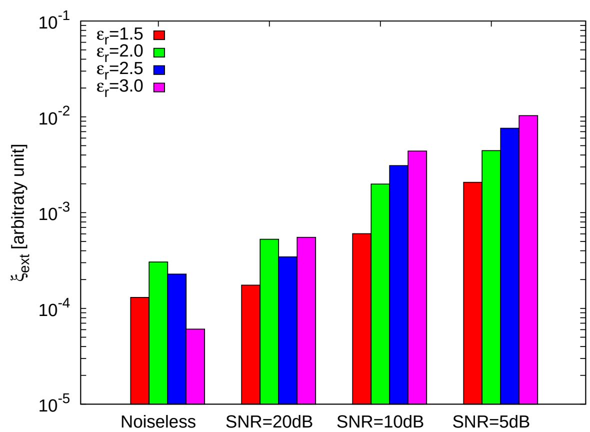

(c)

Figure 26. Behaviour of error figures as a function of ε_r, for different SNR values: (a) total error ξ_{tot}, (b) internal error ξ_{int}, (c) external error ξ_{ext}.

3 TEST CASE: Four Square Cylinders

Goal: show the performances of BCS when dealing with a sparse scatterer

- Number of Views: V
- Number of Measurements: M
- Number of Cells for the Inversion: N
- Number of Cells for the Direct solver: D
- Side of the investigation domain: L

Test Case Description

Direct solver:

- Square domain divided in $\sqrt{D} \times \sqrt{D}$ cells
- Domain side: $L = 3\lambda$
- $D = 1296$ (discretization for the direct solver: $< \lambda/10$)

Investigation domain:

- Square domain divided in $\sqrt{N} \times \sqrt{N}$ cells
- $L = 3\lambda$
- $2ka = 2 \times \frac{2\pi}{\lambda} \times \frac{L\sqrt{2}}{2} = 6\pi\sqrt{2} = 26.65$
- $\#DOF = \frac{(2ka)^2}{2} = \frac{(2\times\frac{2\pi}{\lambda}\times\frac{L\sqrt{2}}{2})^2}{2} = 4\pi^2\left(\frac{L}{\lambda}\right)^2 = 4\pi^2 \times 9 \approx 355.3$
- N scelto in modo da essere vicino a $\#DOF$: $N = 324$ (18×18)

Measurement domain:

- Measurement points taken on a circle of radius $\rho = 3\lambda$
- Full-aspect measurements
- $M \approx 2ka \rightarrow M = 27$

Sources:

- Plane waves
- $V \approx 2ka \rightarrow V = 27$
- Amplitude $A = 1$
- Frequency: 300 MHz $(\lambda = 1)$

Object:

- Four square cylinders of side $\frac{\lambda}{6} = 0.1667$
- $\varepsilon_r \in \{1.5, 2.0, 2.5, 3.0\}$ (two squares), $\varepsilon_r = 1.9$ (two square)
- $\sigma = 0$ [S/m]

BCS parameters:

- Initial estimate of the noise: $n_0 = 1.0 \times 10^{-3}$
- Convergenze parameter: $\tau = 1.0 \times 10^{-8}$

RESULTS: $\varepsilon_r = 1.5$

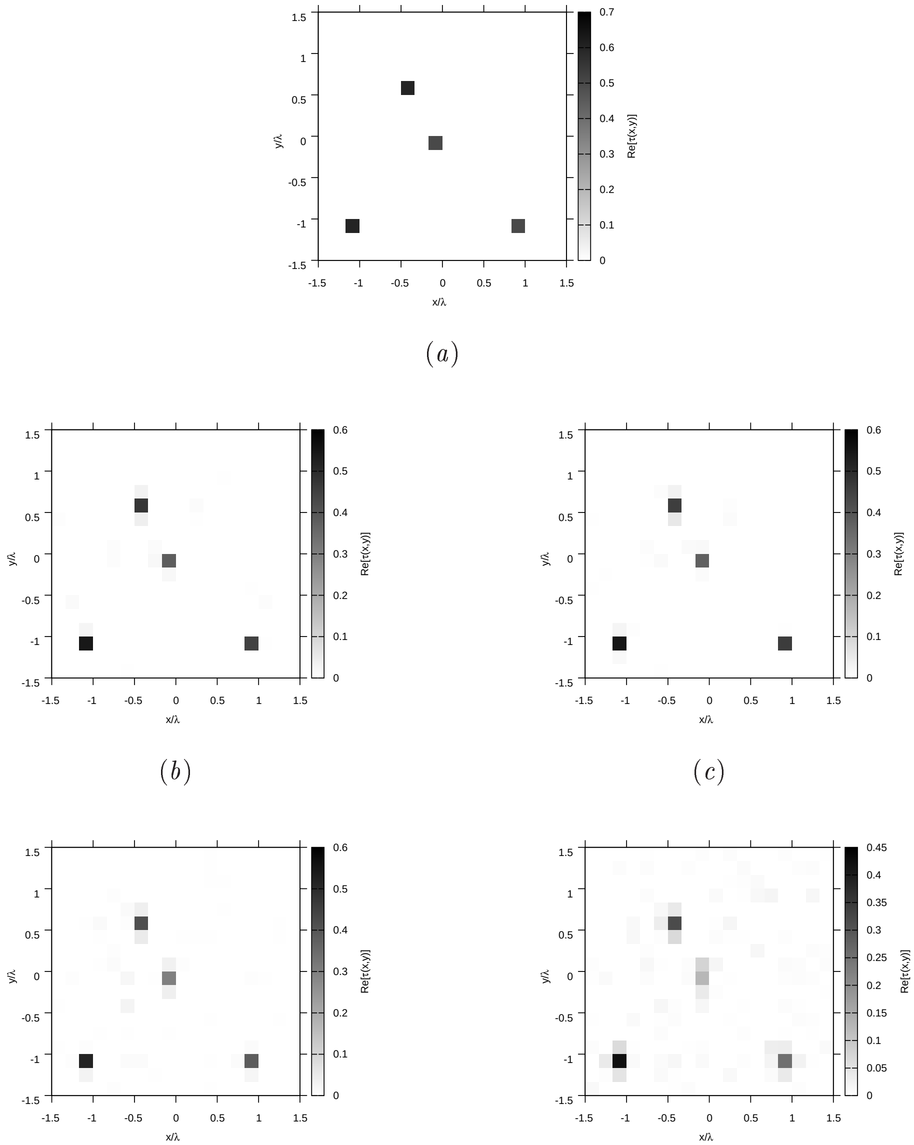

(a)

(b) (c)

(d) (e)

Figure 27. Actual object (a) and BCS reconstructed object for (b) Noiseless case, (c) $SNR = 20$ [dB] , (d) $SNR = 10$ [dB] , (e) $SNR = 5$ [dB].

Observations:

Ricostruzioni molto buone per i casi Noiseless e $SNR = 20\,dB$.

RESULTS: $\varepsilon_r = 2.0$

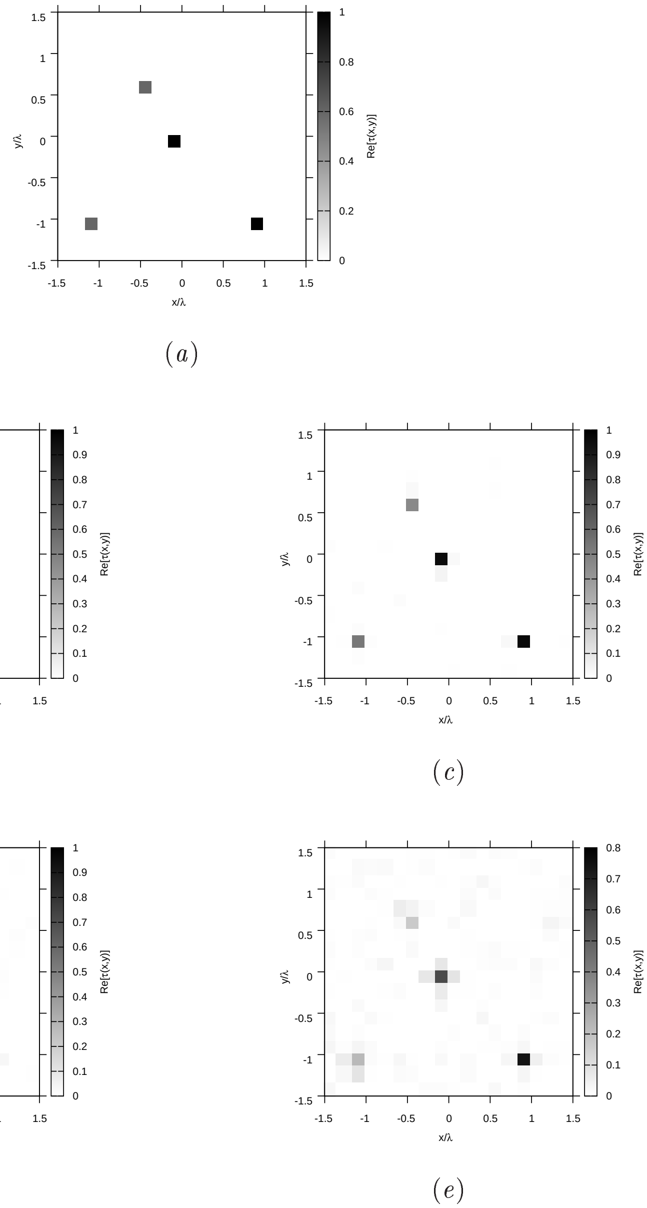

Figure 28. Actual object (a) and BCS reconstructed object for (b) Noiseless case, (c) $SNR = 20$ [dB] , (d) $SNR = 10$ [dB] , (e) $SNR = 5$ [dB].

Observations:

Ricostruzioni molto buone per i casi Noiseless e $SNR = 20\, dB$.

RESULTS: $\varepsilon_r = 2.5$

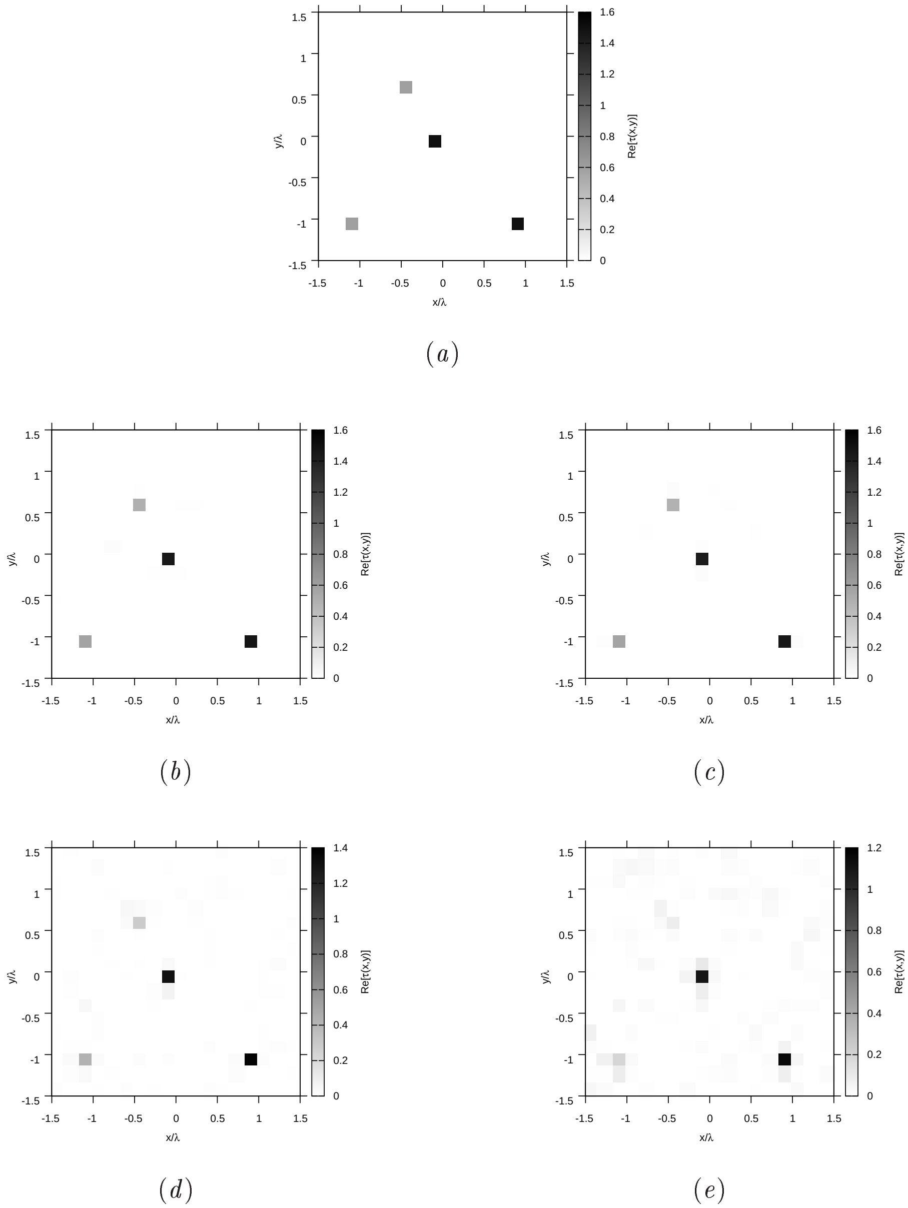

Figure 29. Actual object (a) and BCS reconstructed object for (b) Noiseless case, (c) $SNR = 20$ [dB] , (d) $SNR = 10$ [dB] , (e) $SNR = 5$ [dB].

Observations:

Ricostruzioni molto buone per i casi Noiseless e $SNR = 20\,dB$.

RESULTS: $\varepsilon_r = 3.0$

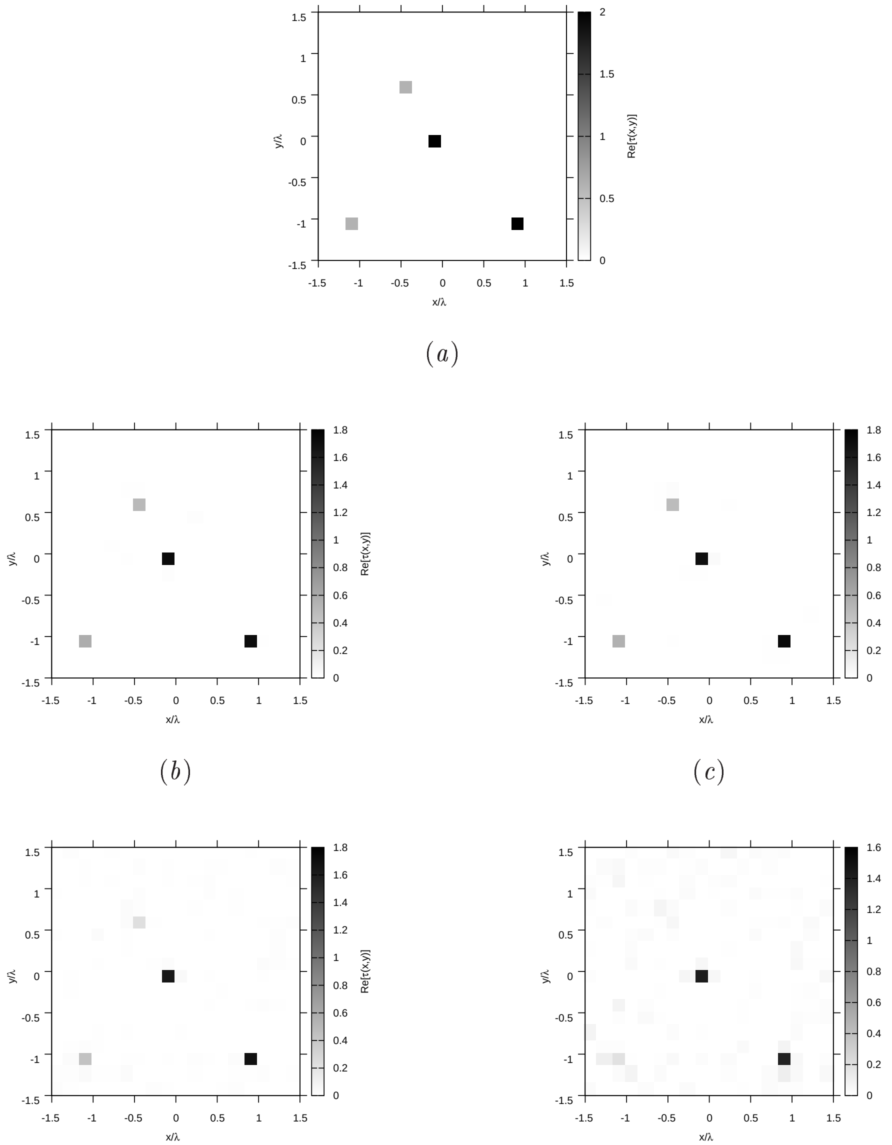

(a) (b) (c) (d) (e)

Figure 30. Actual object (a) and BCS reconstructed object for (b) Noiseless case, (c) $SNR = 20$ [dB] , (d) $SNR = 10$ [dB] , (e) $SNR = 5$ [dB].

Observations:

Ricostruzioni molto buone per i casi Noiseless e $SNR = 20\,dB$.

RESULTS: Error Figures

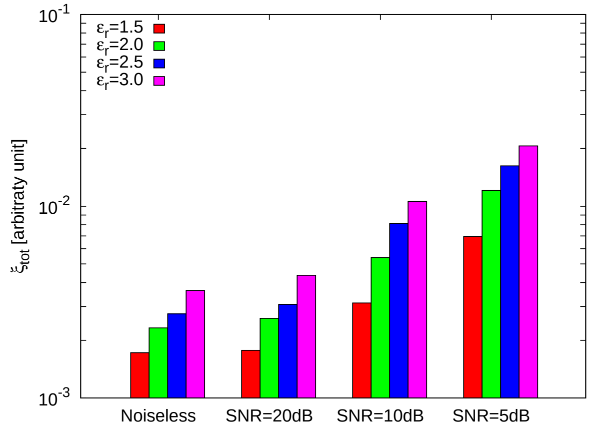

(a)

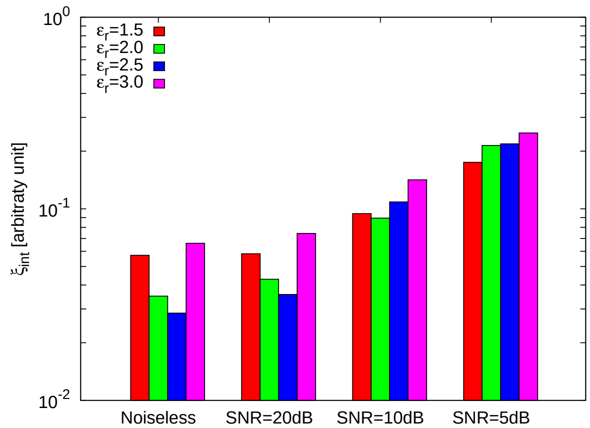

(b)

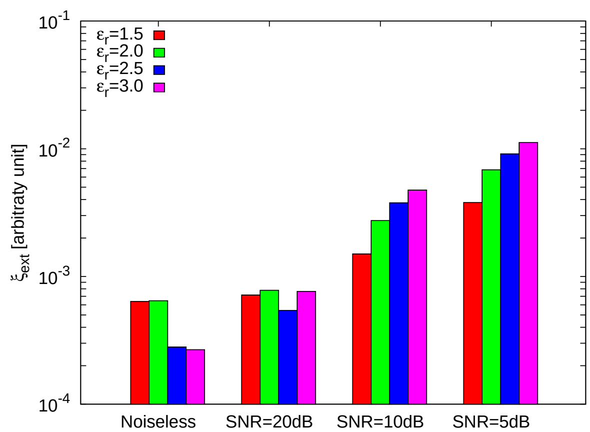

(c)

Figure 31. Behaviour of error figures as a function of ε_r, for different SNR values: (a) total error ξ_{tot}, (b) internal error ξ_{int}, (c) external error ξ_{ext}.

Observations:

Ricostruzioni molto buone per i casi Noiseless e $SNR = 20\,dB$.

4 TEST CASE: Cross-Shaped Cylinder

Goal: show the performances of BCS when dealing with a sparse scatterer

- Number of Views: V
- Number of Measurements: M
- Number of Cells for the Inversion: N
- Number of Cells for the Direct solver: D
- Side of the investigation domain: L

Test Case Description

Direct solver:

- Square domain divided in $\sqrt{D} \times \sqrt{D}$ cells
- Domain side: $L = 3\lambda$
- $D = 1296$ (discretization for the direct solver: $< \lambda/10$)

Investigation domain:

- Square domain divided in $\sqrt{N} \times \sqrt{N}$ cells
- $L = 3\lambda$
- $2ka = 2 \times \frac{2\pi}{\lambda} \times \frac{L\sqrt{2}}{2} = 6\pi\sqrt{2} = 26.65$
- $\#DOF = \frac{(2ka)^2}{2} = \frac{(2 \times \frac{2\pi}{\lambda} \times \frac{L\sqrt{2}}{2})^2}{2} = 4\pi^2 \left(\frac{L}{\lambda}\right)^2 = 4\pi^2 \times 9 \approx 355.3$
- N scelto in modo da essere vicino a $\#DOF$: $N = 324$ (18×18)

Measurement domain:

- Measurement points taken on a circle of radius $\rho = 3\lambda$
- Full-aspect measurements
- $M \approx 2ka \rightarrow M = 27$

Sources:

- Plane waves
- $V \approx 2ka \rightarrow V = 27$
- Amplitude $A = 1$
- Frequency: 300 MHz $(\lambda = 1)$

Object:

- Cross-shaped cylinder
- $\varepsilon_r \in \{1.5, 2.0, 2.5, 3.0\}$
- $\sigma = 0$ [S/m]

BCS parameters:

- Initial estimate of the noise: $n_0 = 1.0 \times 10^{-3}$
- Convergenze parameter: $\tau = 1.0 \times 10^{-8}$

RESULTS: $\varepsilon_r = 1.5$

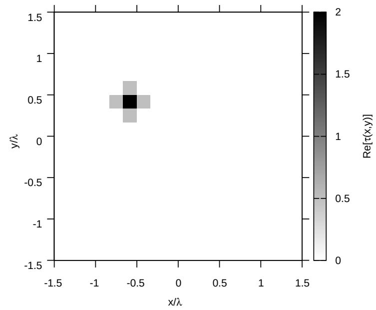

(a)

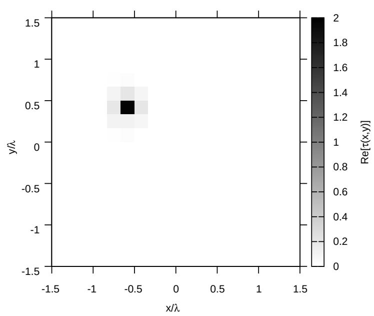

(b)

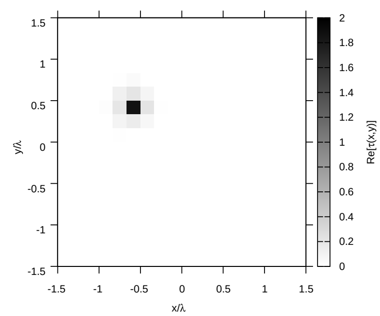

(c)

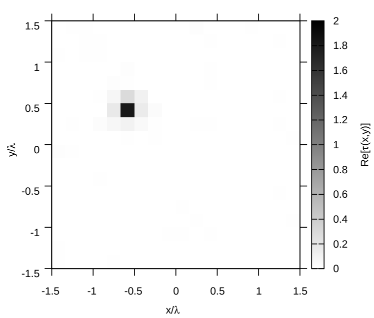

(d)

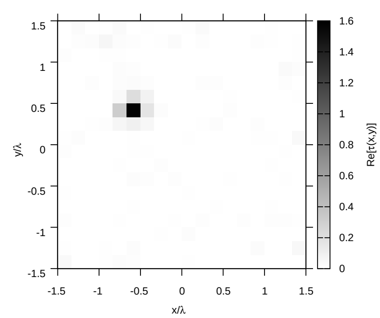

(e)

Figure 32. Actual object (a) and BCS reconstructed object for (b) Noiseless case, (c) $SNR = 20$ [dB] , (d) $SNR = 10$ [dB] , (e) $SNR = 5$ [dB].

Observations:

Ricostruzioni abbastanza buone solo per $\varepsilon_r = 1.5$.

RESULTS: $\varepsilon_r = 2.0$

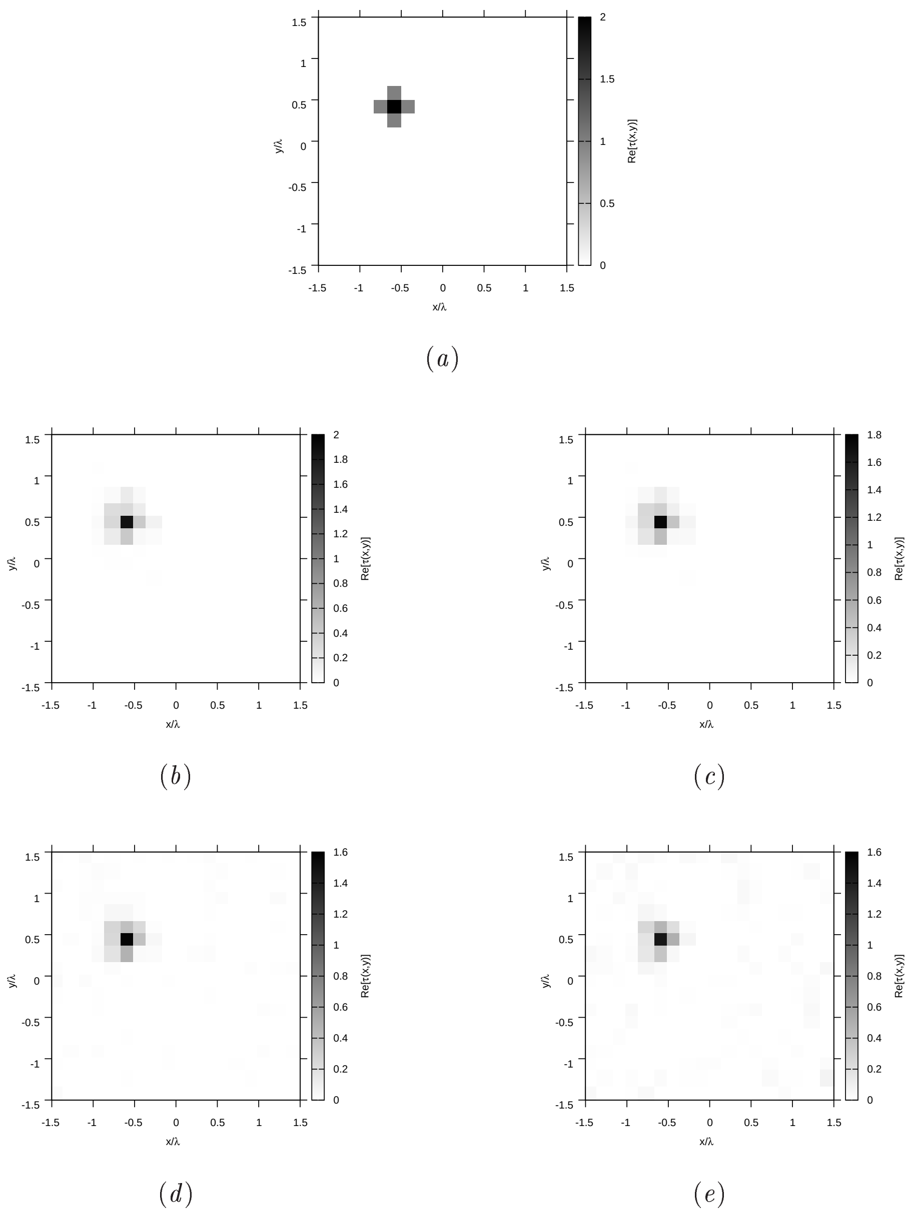

Figure 33. Actual object (a) and BCS reconstructed object for (b) Noiseless case, (c) $SNR = 20$ [dB] , (d) $SNR = 10$ [dB] , (e) $SNR = 5$ [dB].

RESULTS: $\varepsilon_r = 2.5$

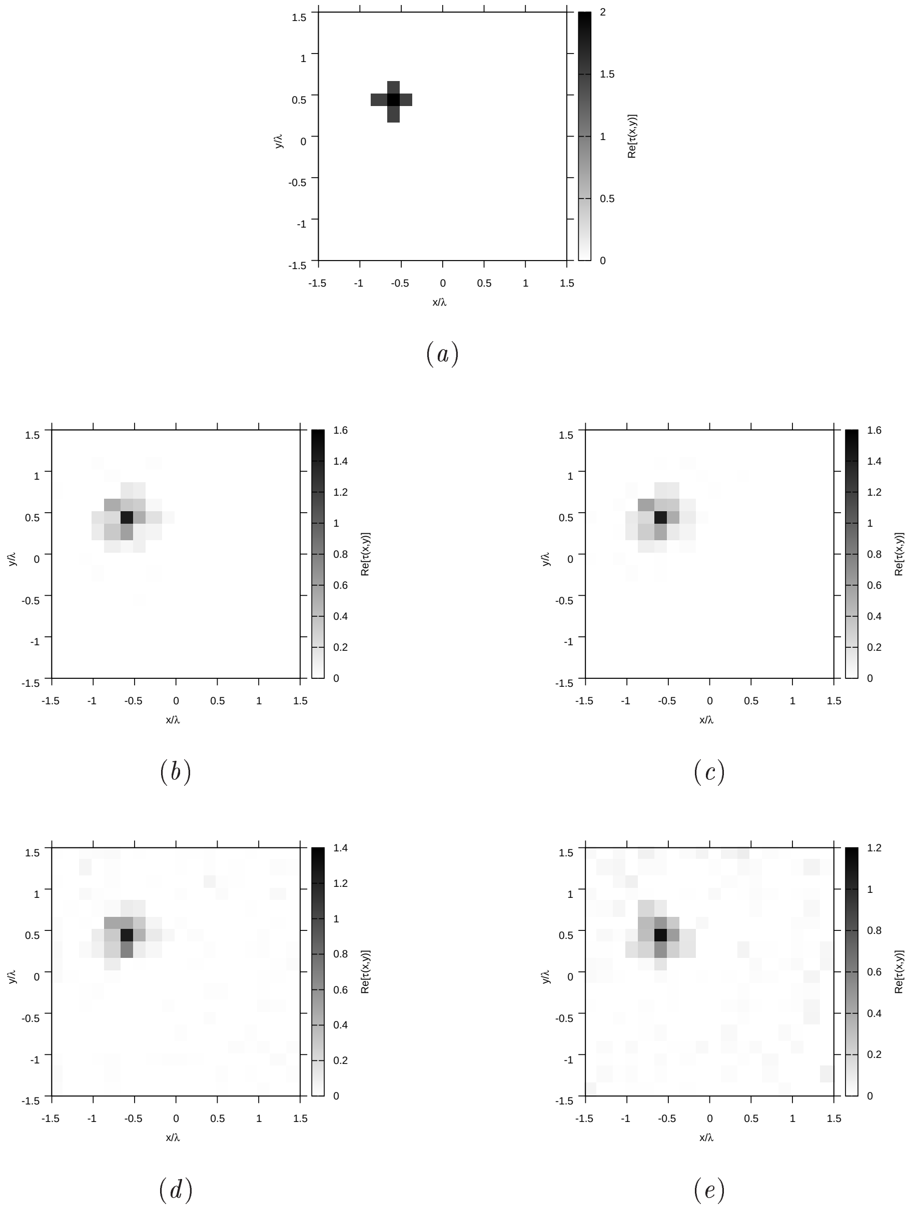

Figure 34. Actual object (a) and BCS reconstructed object for (b) Noiseless case, (c) $SNR = 20$ [dB] , (d) $SNR = 10$ [dB] , (e) $SNR = 5$ [dB].

RESULTS: $\varepsilon_r = 3.0$

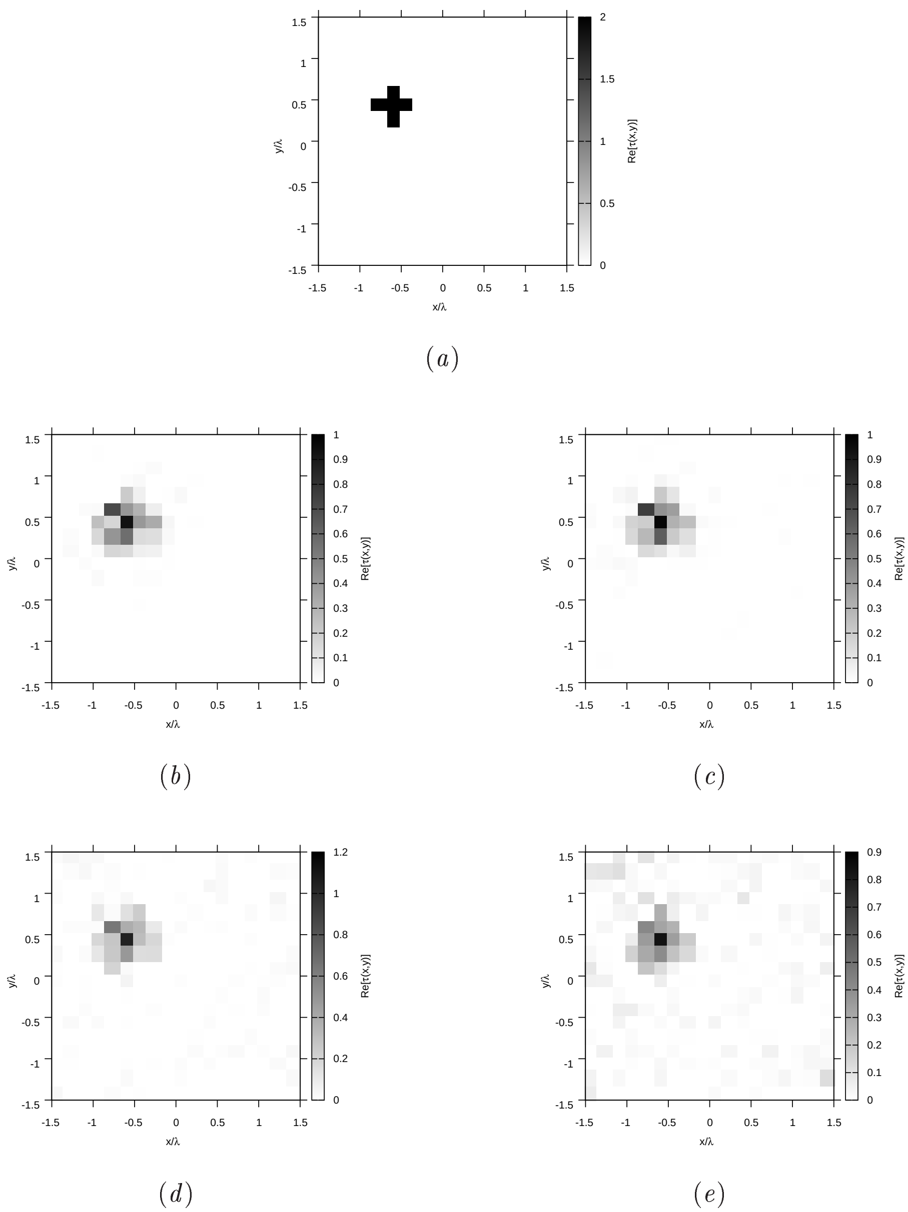

Figure 35. Actual object (a) and BCS reconstructed object for (b) Noiseless case, (c) $SNR = 20$ [dB] , (d) $SNR = 10$ [dB] , (e) $SNR = 5$ [dB].

RESULTS: Error Figures

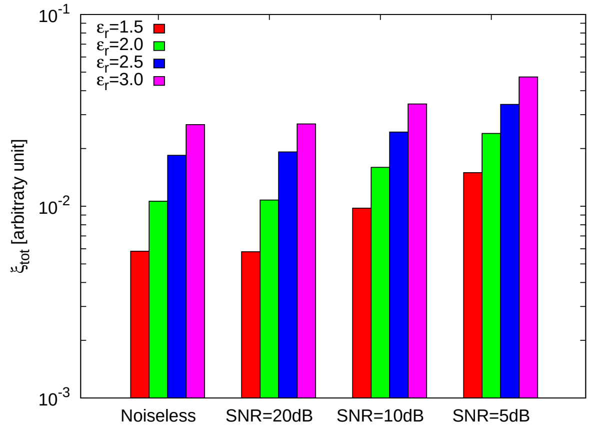

(a)

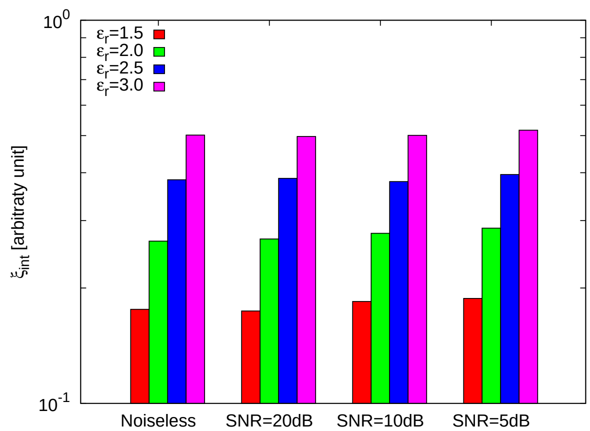

(b)

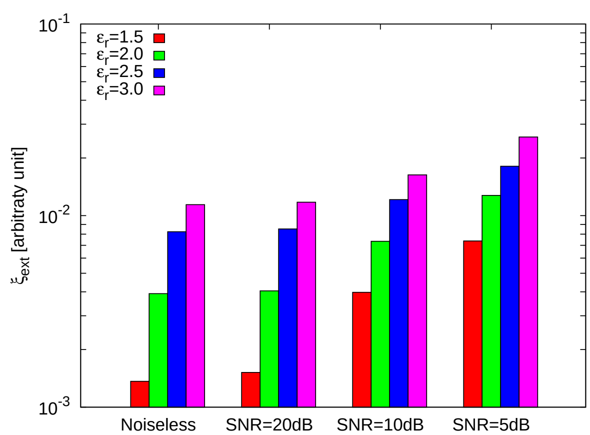

(c)

Figure 36. Behaviour of error figures as a function of ε_r, for different SNR values: (a) total error ξ_{tot}, (b) internal error ξ_{int}, (c) external error ξ_{ext}.

5 TEST CASE: L-Shaped Cylinder

Goal: show the performances of BCS when dealing with a sparse scatterer

- Number of Views: V
- Number of Measurements: M
- Number of Cells for the Inversion: N
- Number of Cells for the Direct solver: D
- Side of the investigation domain: L

Test Case Description

Direct solver:

- Square domain divided in $\sqrt{D} \times \sqrt{D}$ cells
- Domain side: $L = 3\lambda$
- $D = 1296$ (discretization for the direct solver: $< \lambda/10$)

Investigation domain:

- Square domain divided in $\sqrt{N} \times \sqrt{N}$ cells
- $L = 3\lambda$
- $2ka = 2 \times \frac{2\pi}{\lambda} \times \frac{L\sqrt{2}}{2} = 6\pi\sqrt{2} = 26.65$
- $\#DOF = \frac{(2ka)^2}{2} = \frac{(2\times\frac{2\pi}{\lambda}\times\frac{L\sqrt{2}}{2})^2}{2} = 4\pi^2\left(\frac{L}{\lambda}\right)^2 = 4\pi^2 \times 9 \approx 355.3$
- N scelto in modo da essere vicino a $\#DOF$: $N = 324$ (18×18)

Measurement domain:

- Measurement points taken on a circle of radius $\rho = 3\lambda$
- Full-aspect measurements
- $M \approx 2ka \rightarrow M = 27$

Sources:

- Plane waves
- $V \approx 2ka \rightarrow V = 27$
- Amplitude $A = 1$
- Frequency: 300 MHz ($\lambda = 1$)

Object:

- L-shaped cylinder
- $\varepsilon_r \in \{1.5, 2.0, 2.5, 3.0\}$
- $\sigma = 0$ [S/m]

BCS parameters:

- Initial estimate of the noise: $n_0 = 1.0 \times 10^{-3}$
- Convergenze parameter: $\tau = 1.0 \times 10^{-8}$

RESULTS: $\varepsilon_r = 1.5$

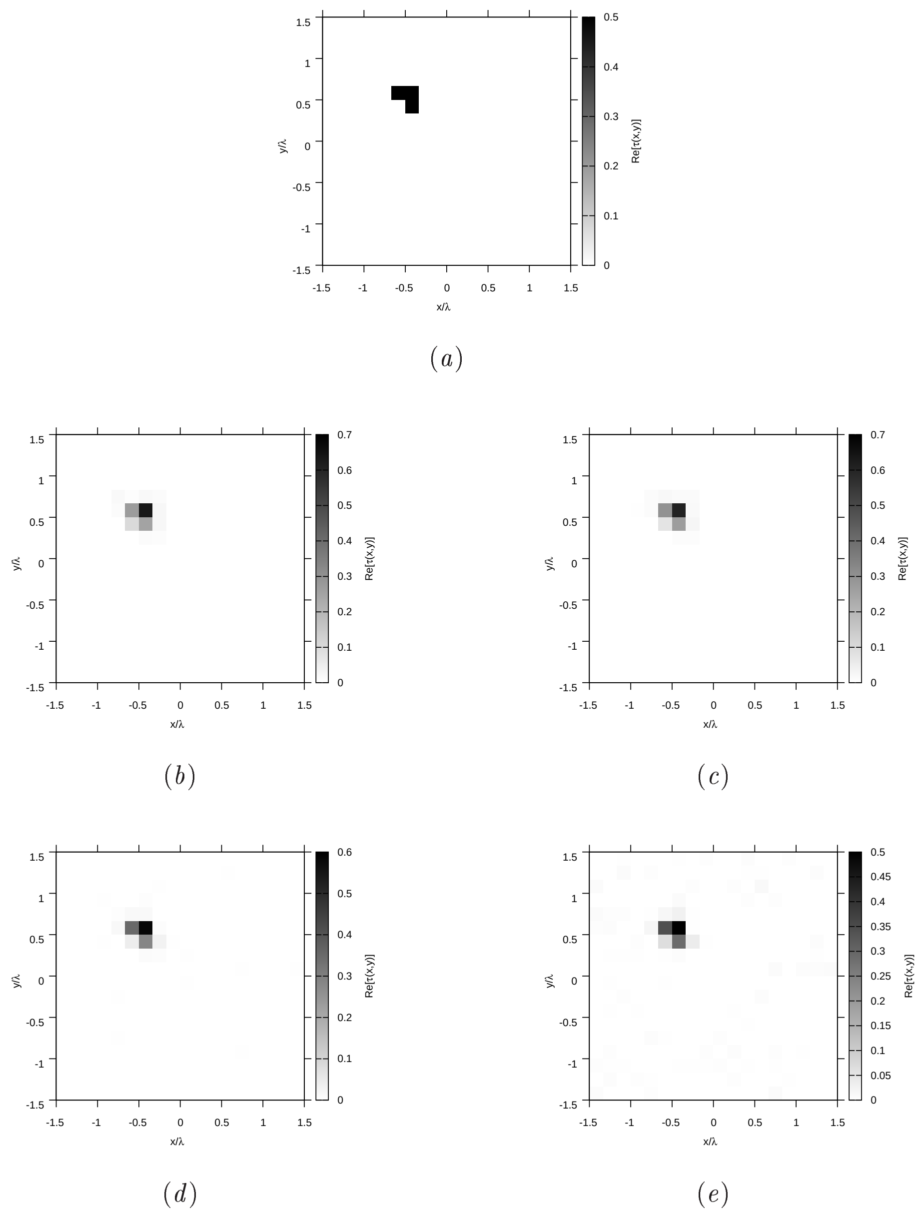

Figure 37. Actual object (a) and BCS reconstructed object for (b) Noiseless case, (c) $SNR = 20$ [dB] , (d) $SNR = 10$ [dB] , (e) $SNR = 5$ [dB].

Observations:

Ricostruzioni abbastanza buone solo per $\varepsilon_r = 1.5$.

RESULTS: $\varepsilon_r = 2.0$

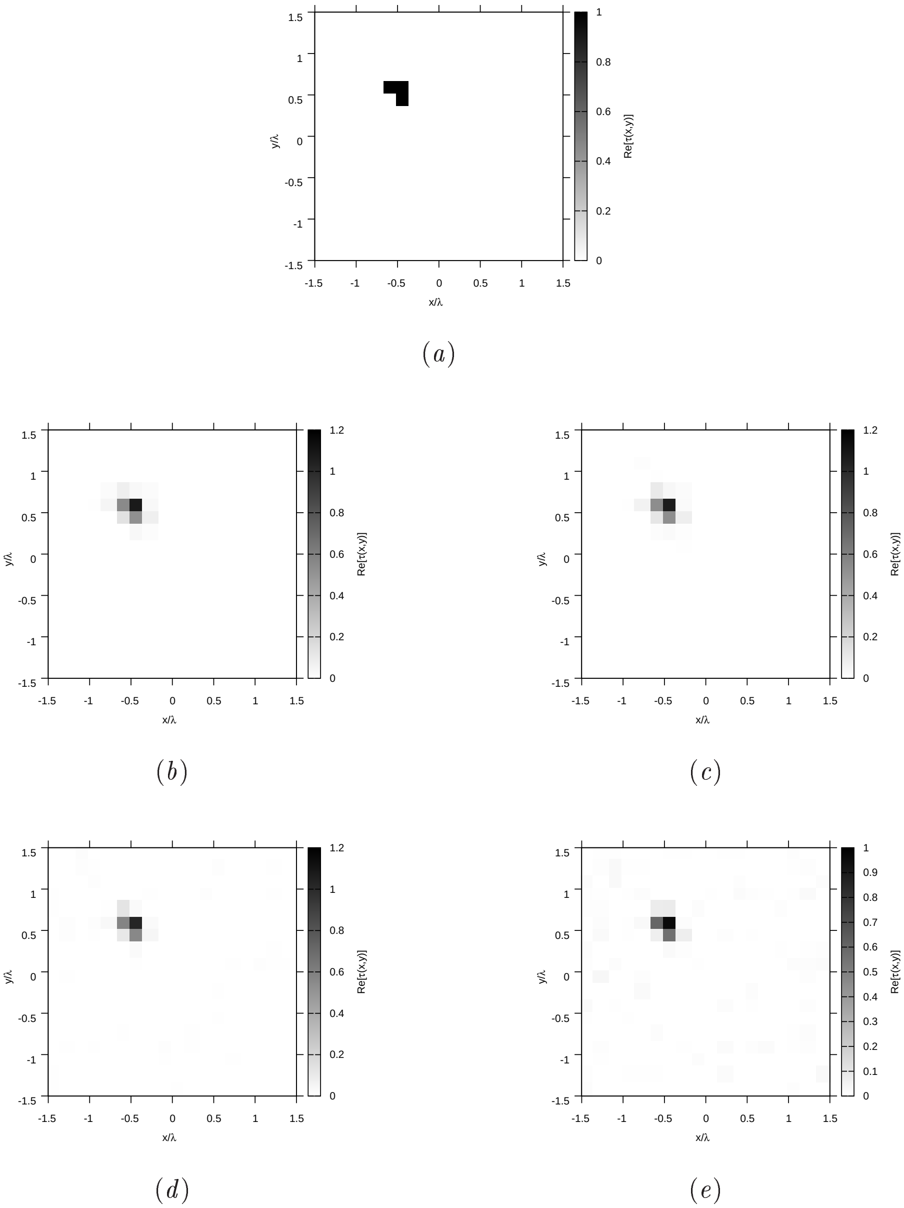

Figure 38. Actual object (a) and BCS reconstructed object for (b) Noiseless case, (c) $SNR = 20$ [dB] , (d) $SNR = 10$ [dB] , (e) $SNR = 5$ [dB].

RESULTS: $\varepsilon_r = 2.5$

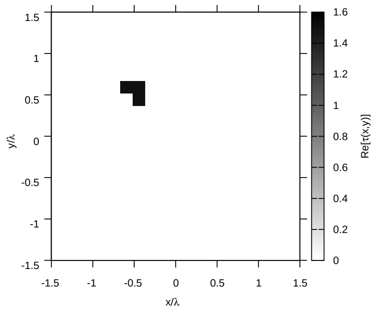

(a)

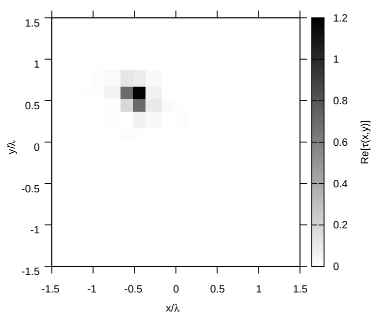

(b)

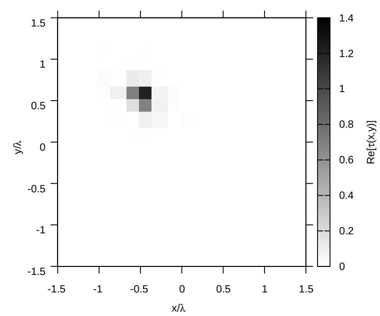

(c)

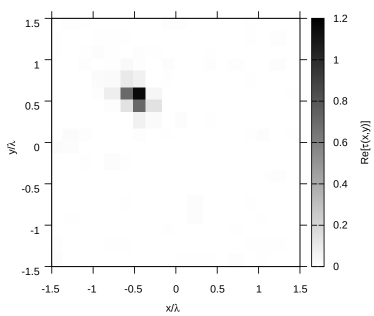

(d)

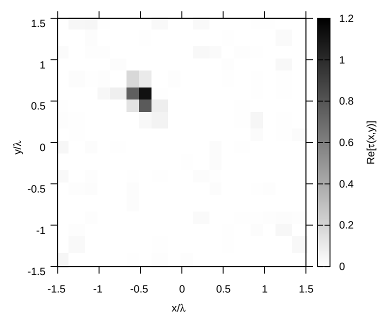

(e)

Figure 39. Actual object (a) and BCS reconstructed object for (b) Noiseless case, (c) $SNR = 20$ [dB] , (d) $SNR = 10$ [dB] , (e) $SNR = 5$ [dB].

RESULTS: $\varepsilon_r = 3.0$

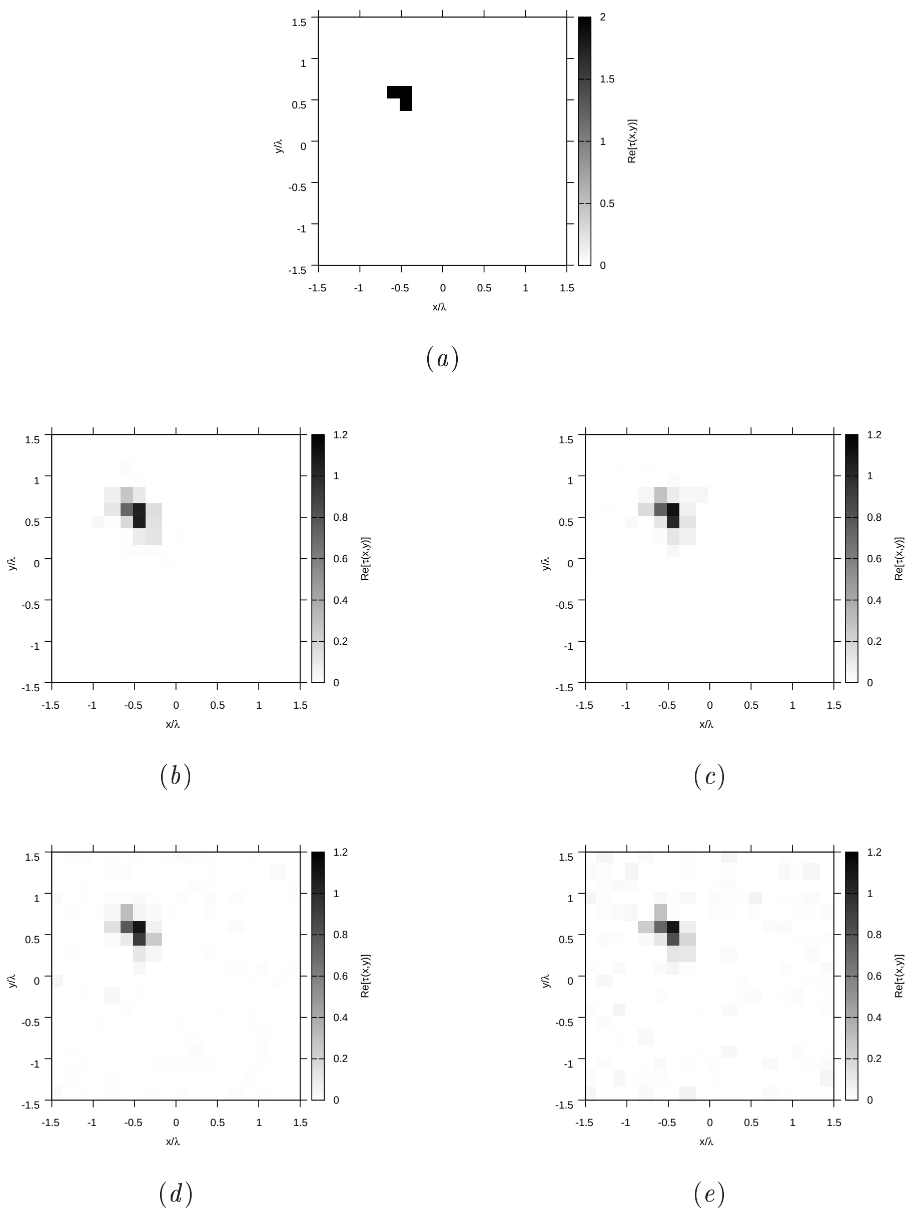

Figure 40. Actual object (a) and BCS reconstructed object for (b) Noiseless case, (c) $SNR = 20$ [dB] , (d) $SNR = 10$ [dB] , (e) $SNR = 5$ [dB].

RESULTS: Error Figures

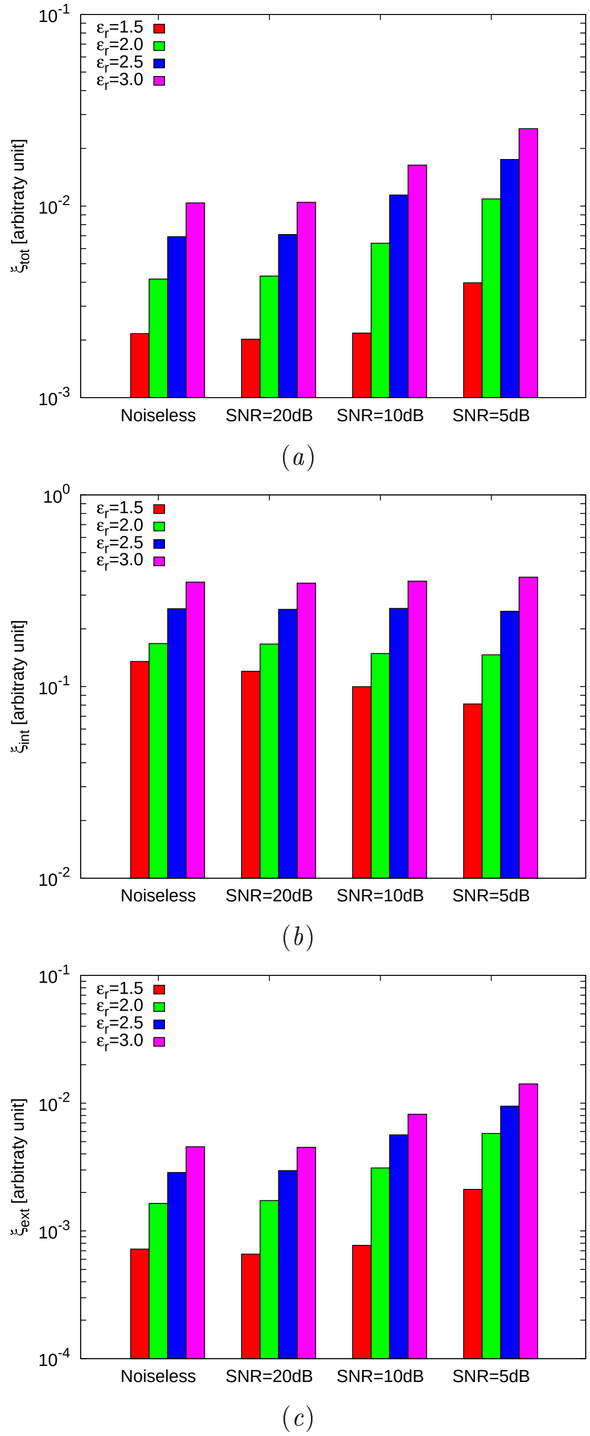

Figure 41. Behaviour of error figures as a function of ε_r, for different SNR values: (a) total error ξ_{tot}, (b) internal error ξ_{int}, (c) external error ξ_{ext}.

6 TEST CASE: Inhomogeneous L-Shaped Cylinder

Goal: show the performances of BCS when dealing with a sparse scatterer

- Number of Views: V
- Number of Measurements: M
- Number of Cells for the Inversion: N
- Number of Cells for the Direct solver: D
- Side of the investigation domain: L

Test Case Description

Direct solver:

- Square domain divided in $\sqrt{D} \times \sqrt{D}$ cells
- Domain side: $L = 3\lambda$
- $D = 1296$ (discretization for the direct solver: $< \lambda/10$)

Investigation domain:

- Square domain divided in $\sqrt{N} \times \sqrt{N}$ cells
- $L = 3\lambda$
- $2ka = 2 \times \frac{2\pi}{\lambda} \times \frac{L\sqrt{2}}{2} = 6\pi\sqrt{2} = 26.65$
- $\#DOF = \frac{(2ka)^2}{2} = \frac{(2\times\frac{2\pi}{\lambda}\times\frac{L\sqrt{2}}{2})^2}{2} = 4\pi^2\left(\frac{L}{\lambda}\right)^2 = 4\pi^2 \times 9 \approx 355.3$
- N scelto in modo da essere vicino a $\#DOF$: $N = 324$ (18×18)

Measurement domain:

- Measurement points taken on a circle of radius $\rho = 3\lambda$
- Full-aspect measurements
- $M \approx 2ka \rightarrow M = 27$

Sources:

- Plane waves
- $V \approx 2ka \rightarrow V = 27$
- Amplitude $A = 1$
- Frequency: 300 MHz ($\lambda = 1$)

Object:

- Inhomogeneous L-shaped cylinder
- $\varepsilon_r \in \{1.5, 2.0, 2.5, 3.0\}$
- $\sigma = 0$ [S/m]

BCS parameters:

- Initial estimate of the noise: $n_0 = 1.0 \times 10^{-3}$
- Convergenze parameter: $\tau = 1.0 \times 10^{-8}$

RESULTS: $\varepsilon_r = 1.5$

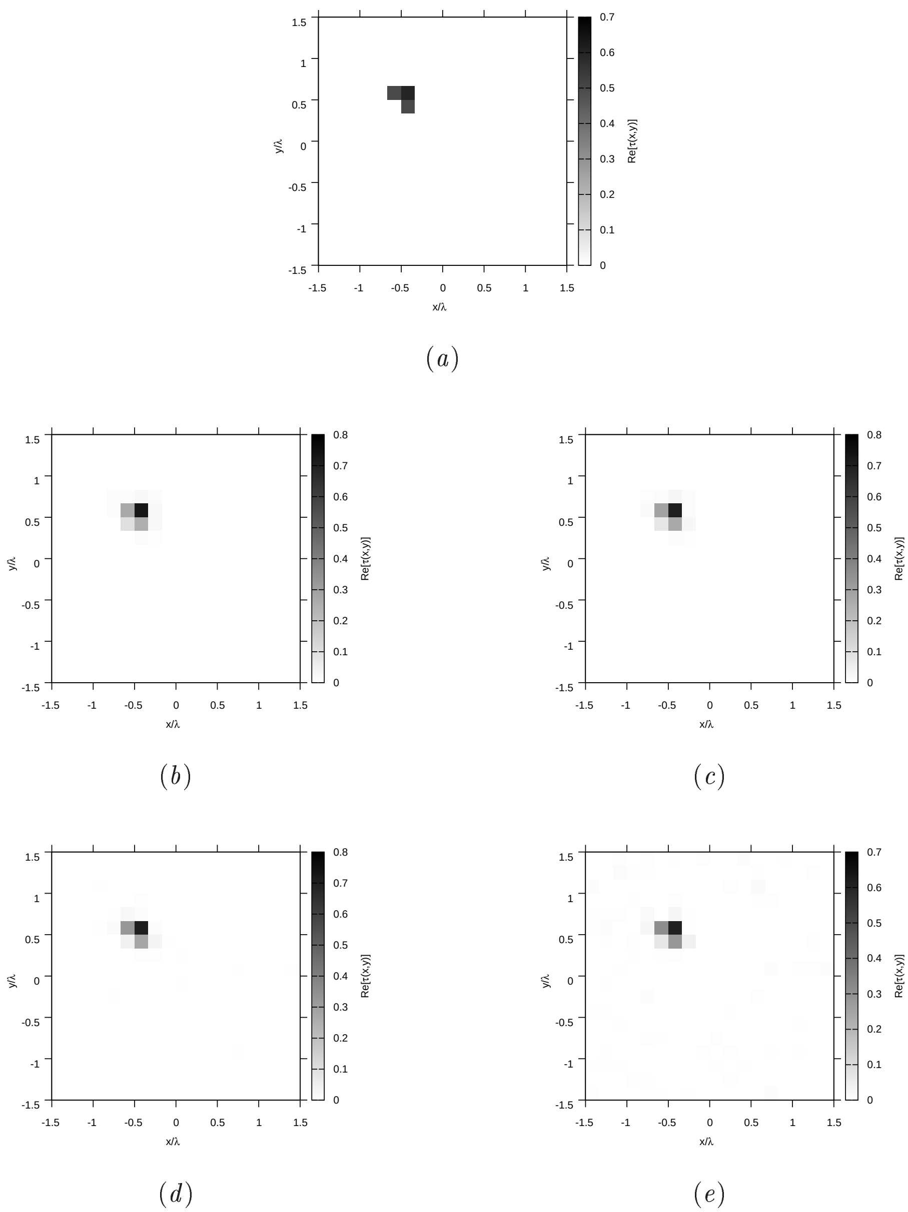

Figure 42. Actual object (a) and BCS reconstructed object for (b) Noiseless case, (c) $SNR = 20$ [dB] , (d) $SNR = 10$ [dB] , (e) $SNR = 5$ [dB].

Observations:

Ricostruzioni abbastanza buone solo per $\varepsilon_r = 1.5$.

RESULTS: $\varepsilon_r = 2.0$

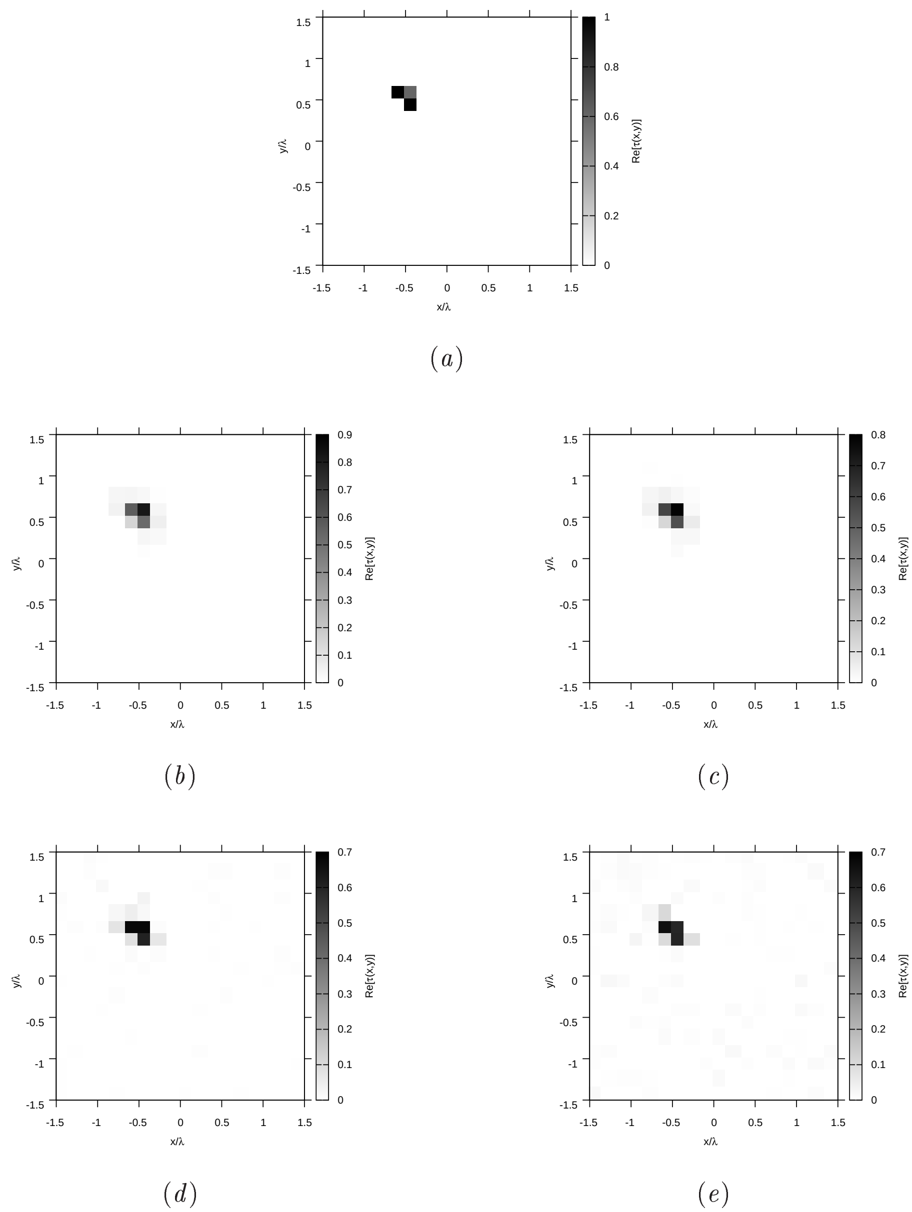

Figure 43. Actual object (a) and BCS reconstructed object for (b) Noiseless case, (c) $SNR = 20$ [dB] , (d) $SNR = 10$ [dB] , (e) $SNR = 5$ [dB].

RESULTS: $\varepsilon_r = 2.5$

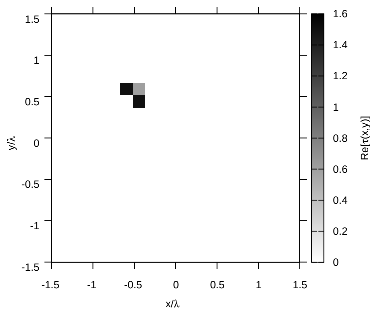

(a)

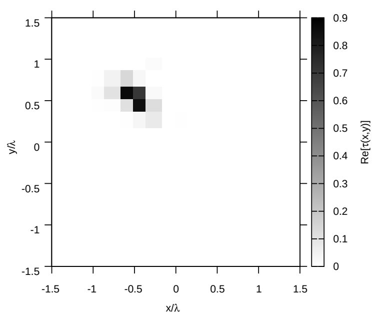

(b)

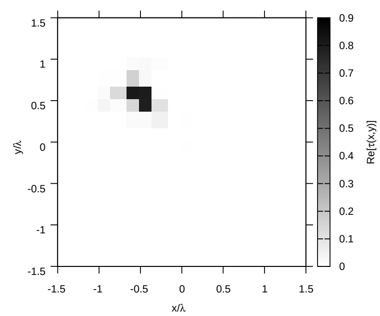

(c)

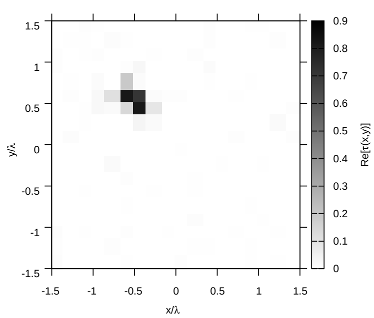

(d)

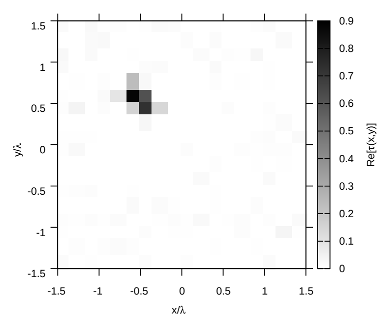

(e)

Figure 44. Actual object (a) and BCS reconstructed object for (b) Noiseless case, (c) $SNR = 20$ [dB] , (d) $SNR = 10$ [dB] , (e) $SNR = 5$ [dB].

RESULTS: $\varepsilon_r = 3.0$

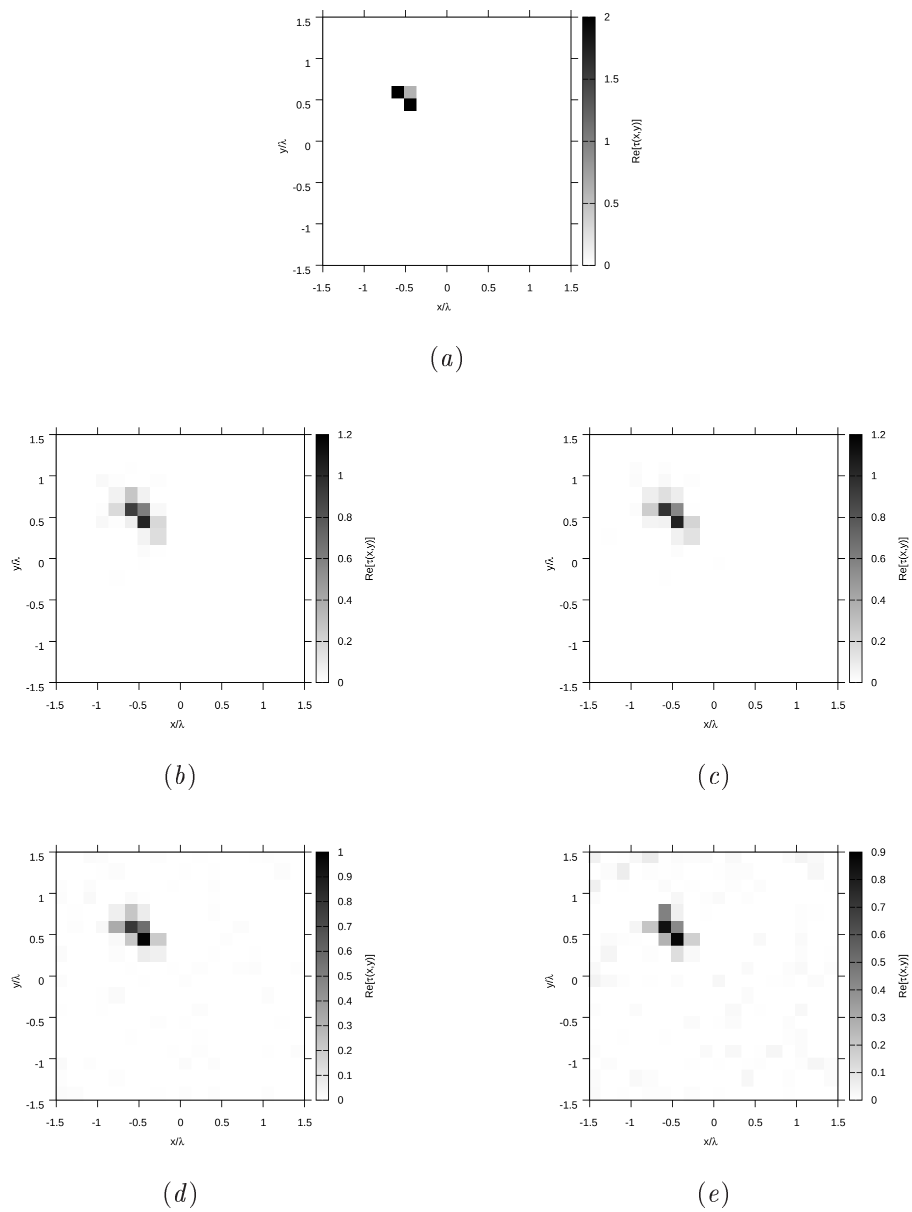

Figure 45. Actual object (a) and BCS reconstructed object for (b) Noiseless case, (c) $SNR = 20$ [dB] , (d) $SNR = 10$ [dB] , (e) $SNR = 5$ [dB].

RESULTS: Error Figures

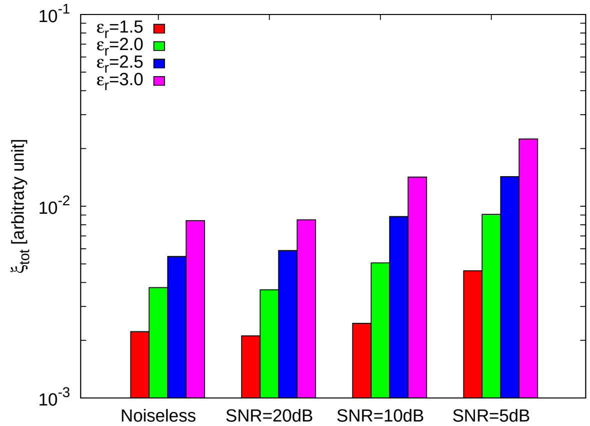

(a)

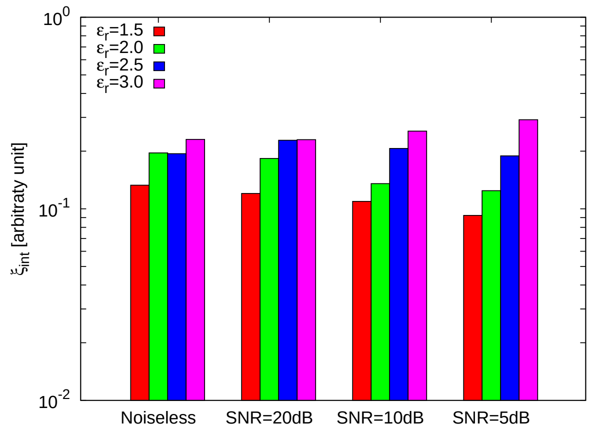

(b)

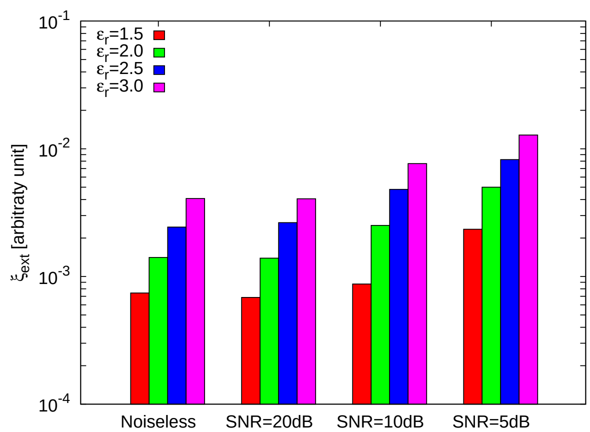

(c)

Figure 46. Behaviour of error figures as a function of ε_r, for different SNR values: (a) total error ξ_{tot}, (b) internal error ξ_{int}, (c) external error ξ_{ext}.

References

[1] E. J. Candes and M. B. Wakin, "An introduction to compressive sampling", *IEEE Signal Processing Magazine*, vol. 25, no. 2, pp. 21-30, March 2008.

[2] S. Ji, Y. Xue, and L. Carin, "Bayesian compressive sampling", *IEEE Trans. on Signal Processing*, vol. 56, no. 6, pp. 2346-2356, June 2008.

[3] R. F. Harrington, *Field computation by moment methods*, New York: IEEE Press, 1993.

[4] J. H. Richmond, "Scattering by a dielectric cylinder of arbitrary cross shape", *IEEE Trans. Antennas Propagat.*, vol. AP-13, no. 3, pp. 334-341, May 1965.

[5] M. Slaney, A. C. Kak, and L. E. Larsen, "Limitations of imaging with first-order diffraction tomography", *IEEE Trans. on Microwave Theory and Techniques*, vol. MTT-32, no. 8, pp. 860-874, Aug. 1984.

[6] L. Poli, G. Oliveri, and A. Massa, "Imaging sparse metallic cylinders through a Local Shape Function Bayesian Compressive Sensing approach," Journal of Optical Society of America A, vol. 30, no. 6, pp. 1261-1272, 2013.

[7] F. Viani, L. Poli, G. Oliveri, F. Robol, and A. Massa, "Sparse scatterers imaging through approximated multitask compressive sensing strategies," Microwave Opt. Technol. Lett., vol. 55, no. 7, pp. 1553-1558, Jul. 2013.

[8] L. Poli, G. Oliveri, P. Rocca, and A. Massa, "Bayesian compressive sensing approaches for the reconstruction of two-dimensional sparse scatterers under TE illumination," IEEE Trans. Geosci. Remote Sensing, vol. 51, no. 5, pp. 2920-2936, May. 2013.

[9] L. Poli, G. Oliveri, and A. Massa, "Microwave imaging within the first-order Born approximation by means of the contrast-field Bayesian compressive sensing," IEEE Trans. Antennas Propag., vol. 60, no. 6, pp. 2865-2879, Jun. 2012.

[10] G. Oliveri, P. Rocca, and A. Massa, "A bayesian compressive sampling-based inversion for imaging sparse scatterers," IEEE Trans. Geosci. Remote Sensing, vol. 49, no. 10, pp. 3993-4006, Oct. 2011.

[11] G. Oliveri, L. Poli, P. Rocca, and A. Massa, "Bayesian compressive optical imaging within the Rytov approximation," Optics Letters, vol. 37, no. 10, pp. 1760-1762, 2012.

[12] L. Poli, G. Oliveri, F. Viani, and A. Massa, âMT-BCS-based microwave imaging approach through minimum-norm current expansion,â IEEE Trans. Antennas Propag., in press. doi:10.1109/TAP.2013.2265254

[13] S. C. Hagness, E. C. Fear, and A. Massa, "Guest Editorial: Special Cluster on Microwave Medical Imaging", IEEE Antennas Wireless Propag. Lett., vol. 11, pp. 1592-1597, 2012.

[14] G. Oliveri, Y. Zhong, X. Chen, and A. Massa, "Multi-resolution subspace-based optimization method for inverse scattering," Journal of Optical Society of America A, vol. 28, no. 10, pp. 2057-2069, Oct. 2011.

[15] A. Randazzo, G. Oliveri, A. Massa, and M. Pastorino, "Electromagnetic inversion with the multiscaling inexact-Newton method - Experimental validation," Microwave Opt. Technol. Lett., vol. 53, no. 12, pp. 2834-2838, Dec. 2011.

[16] G. Oliveri, L. Lizzi, M. Pastorino, and A. Massa, "A nested multi-scaling inexact-Newton iterative approach for microwave imaging," IEEE Trans. Antennas Propag., vol. 60, no. 2, pp. 971-983, Feb. 2012.

[17] G. Oliveri, A. Randazzo, M. Pastorino, and A. Massa, "Electromagnetic imaging within the contrast-source formulation by means of the multiscaling inexact Newton method," Journal of Optical Society of America A, vol. 29, no. 6, pp. 945-958, 2012.

[18] M. Benedetti, D. Lesselier, M. Lambert, and A. Massa, "Multiple shapes reconstruction by means of multi-region level sets," IEEE Trans. Geosci. Remote Sensing, vol. 48, no. 5, pp. 2330-2342, May 2010.

[19] M. Benedetti, D. Lesselier, M. Lambert, and A. Massa, "A multi-resolution technique based on shape optimization for the reconstruction of homogeneous dielectric objects," Inverse Problems, vol. 25, no. 1, pp. 1-26, Jan. 2009.

[20] M. Donelli, D. Franceschini, P. Rocca, and A. Massa, "Three-dimensional microwave imaging problems solved through an efficient multi-scaling particle swarm optimization," IEEE Trans. Geosci. Remote Sensing, vol. 47, no. 5, pp. 1467-1481, May 2009.

[21] M. Benedetti, G. Franceschini, R. Azaro, and A. Massa, "A numerical assessment of the reconstruction effectiveness of the integrated GA-based multicrack strategy," IEEE Antennas Wireless Propag. Lett., vol. 6, pp. 271-274, 2007.

[22] P. Rocca, M. Carlin, G. Oliveri, and A. Massa, "Interval analysis as applied to inverse scattering," IEEE International Symposium on Antennas Propag. (APS/URSI 2013), Chicago, Illinois, USA, Jul. 8-14, 2012.

[23] L. Manica, P. Rocca, M. Salucci, M. Carlin, and A. Massa, "Scattering data inversion through interval analysis under Rytov approximation," 7th European Conference on Antennas Propag. (EuCAP 2013), Gothenburg, Sweden, Apr. 8-12, 2013.

[24] P. Rocca, M. Carlin, and A. Massa, "Imaging weak scatterers by means of an innovative inverse scattering technique based on the interval analysis," 6th European Conference on Antennas Propag. (EuCAP 2012), Prague, Czech Republic, Mar. 26-30, 2012.

[25] G. Oliveri and A. Massa, "Bayesian compressive sampling for pattern synthesis with maximally sparse non-uniform linear arrays," IEEE Trans. Antennas Propag., vol. 59, no. 2, pp. 467-481, Feb. 2011.

[26] G. Oliveri, M. Carlin, and A. Massa, "Complex-weight sparse linear array synthesis by Bayesian Compressive Sampling," IEEE Trans. Antennas Propag., vol. 60, no. 5, pp. 2309-2326, May 2012.

[27] G. Oliveri, P. Rocca, and A. Massa, "Reliable Diagnosis of Large Linear Arrays - A Bayesian Compressive Sensing Approach," IEEE Trans. Antennas Propag., vol. 60, no. 10, pp. 4627-4636, Oct. 2012.

[28] F. Viani, G. Oliveri, and A. Massa, âCompressive sensing pattern matching techniques for synthesizing planar sparse arraysâ IEEE Trans. Antennas Propag., in press. doi:10.1109/TAP.2013.2267195

[29] M. Carlin, P. Rocca, G. Oliveri, F. Viani, and A. Massa, "Directions-of-Arrival Estimation through Bayesian Compressive Sensing strategies," IEEE Trans. Antennas Propag., in press.

[30] M. Carlin, P. Rocca, "A Bayesian compressive sensing strategy for direction-of-arrival estimation," 6th European Conference on Antennas Propag. (EuCAP 2012), Prague, Czech Republic, pp. 1508-1509, 26-30 Mar. 2012.

[31] M. Carlin, P. Rocca, G. Oliveri, and A. Massa, âBayesian compressive sensing as applied to directions-of-arrival estimation in planar arraysâ, Journal of Electrical and Computer Engineering, Special Issue on âAdvances in Radar Technologiesâ, in press.